

DISSERTATION

submitted to the

Combined Faculties for the Natural Sciences and for Mathematics

of the Ruperto-Carola University of Heidelberg, Germany

for the degree of

Doctor of Natural Sciences

presented by

Diplom-Bioinformatiker(FH) Tim Maiwald

born in Mönchengladbach, Germany

Oral examination:

*COMPUTATIONAL ANALYSIS OF THE INTERFERON ALPHA SIGNALLING PATHWAY
USING A SYSTEMS BIOLOGY MODELLING APPROACH*

Referees: Prof. Dr. Ursula Kummer

Prof. Dr. Rainer Zawatzky

Imagination is more important than knowledge. For knowledge is limited, whereas imagination embraces the entire world, stimulating progress, giving birth to evolution.

Albert Einstein, 1931

Acknowledgments

First of all, I'd like to thank my supervisor Prof. Ursula Kummer for giving me the opportunity to work on this project. Her scientific support during my PhD was outstanding and her voice of reason was encouraging throughout every aspect of this project.

I thank Prof. Rainer Zawatzky for being the second referee for this thesis. His expertise has always been a great addition to our collaboration.

I'm grateful to Prof. Ursula Klingmüller for her intense support towards this project and for readily offering me any help required.

I'd like to thank all members of my group for the nice time we had together. Especially, I want to thank Katrin, for being the "Postdoc of Trust" throughout my time in the group; Sven and Ralph for their technical help and theoretical expertise; Jennifer for the nice coffee-breaks and fruitful discussions and Irina and Natalia for their collaborative support.

Also, I'm grateful to all members of the Klingmüller group for lunch breaks and generally being friendly to me. I'd like to highlight Annette Schneider, without whom this project would not have been possible. Personally and scientifically, she has been an excellent collaborative partner. Thanks for everything. Furthermore, I'd like to thank Marcel for his theoretical expertise that he readily shared and Katharina for her enthusiastic approach towards our collaboration. I thank former group members Verena Becker and Julie Bachmann for fruitful discussion and entertaining coffee breaks.

I'd like to thank Andreas Raue for fruitful discussions and technical support that he readily offered on multiple occasions.

I thank Simone Rosenberger for fruitful discussions and her strong-willed approach to obstacles.

I'm grateful to Hauke Busch for his versatile collaborative support towards this project.

Finally, I'd like to thank my family, friends and Simone for their great support and always being there for me during the good and difficult times of my PhD project.

Summary.....	2
Zusammenfassung.....	3
Publications.....	4
Introduction	5
Interferon Subtypes.....	5
Interferon alpha signalling through JAK/STAT pathway	6
Missing Links & Medical impact	9
Systems Biology	11
Modelling	12
Aim of the Study	13
Results	14
Modelling of the IFN alpha signalling pathway	14
Model description.....	15
Hypothesis: IRF9 overexpression amplifies signalling kinetics	23
Proving further impact of IRF9 concentration through experimental measurements.....	30
Understanding the diverse genetic response through a bioinformatics approach	34
Model reduction and parameter estimation	36
Discussion.....	56
Identification of key molecules and reactions of the IFN alpha pathway	56
Analysis of genetic response pattern	58
Medical impact.....	59
Sensitivity-based model reduction and parameter estimation.....	60
Time Scale separation based model reduction and parameter estimation.....	62
Materials & Methods.....	64
Modelling	64
Sensitivity based model reduction.....	67
Time scale separation based model reduction	68
String Database	70
Estimation of gene induction times.....	71
Abbreviations	72
Citations	74
Erklärung.....	85

SUMMARY

In this thesis, signalling dynamics of the interferon alpha stimulated JAK/STAT pathway have been studied using a computational modelling approach. A model simulating the kinetic response of an interferon alpha stimulated Huh7.5 cell was developed using literature data and experimental measurements. The model was used for predictions regarding the kinetic behaviour of the signal transduction. IRF-9, a transcription factor necessary for the transcriptionally active ISGF-3 complex, was predicted to be a major contributor to the time dependent kinetic behaviour of the interferon alpha stimulated signal transduction. An overexpression of IRF-9 was predicted to enhance and accelerate the anti-viral response following interferon alpha stimulation. Furthermore, constitutive negative feedback by nuclear phosphatases and induced negative feedback by SOCS proteins were predicted to have a major impact on the JAK/STAT signalling pathway. Additionally, phosphatase protection of the ISGF-3 complex by DNA binding was proposed to be necessary for the observed kinetic measurements. Predictions regarding IRF-9 were validated by experimental measurements comparing wild-type cells to IRF-9 overexpression cells. Both cell lines showed the predicted behaviour after interferon alpha stimulation for active signal transducers.

Furthermore, the effect was observed on a genetic level, as an array experiment showed upregulation and acceleration of prominent anti-viral genes such as Mx1 in the IRF-9 overexpressing cells in comparison to the wild-type environment. Therefore, overexpression of IRF-9 was identified as a method to enhance the JAK/STAT signalling pathway.

A bioinformatical approach was used to predict underlying mechanisms controlling individual gene induction patterns observed in the array experiment. Results showed that hub-gene IRF1 could be involved in a transcriptional network controlling early and late anti-viral responses following interferon alpha stimulation.

To improve model predictions and to identify key reactions for additional experimental design, a two-phase model reduction and parameter estimation approaches were performed. For the first reduction, the model was decreased from 61 free parameters to 33 free parameters. After a parameter fitting approach, the model retained its ability to accurately fit the experimental data. Furthermore, the second model reduction lead to a minimal model with 22 free parameters, which was able to fit the experimental data well.

ZUSAMMENFASSUNG

In dieser Dissertation wurde die Signaltransduktion des durch Interferon-Alpha stimulierten JAK/STAT Signalweges durch die Verwendung eines systembiologischen Modelling Ansatzes studiert. Ein Modell, das die kinetische Reaktion einer Interferon-Alpha stimulierten Huh7.5 Zelle abbildet, wurde unter Zuhilfenahme von experimentellen Messungen und publizierten Daten entwickelt. Mit Hilfe des Modells wurden Vorhersagen über das kinetische Verhalten der Signaltransduktion getätigt: Die Konzentration von IRF-9, ein Transkriptionsfaktor der Bestandteil des transkriptionell-aktiven ISGF-3 Komplexes ist, wurde durch die Analyse als wesentlicher Einfluss auf das zeitabhängige kinetische Verhalten des JAK/STAT Signalweg prognostiziert. Eine Überexpression von IRF-9 sollte demnach eine Beschleunigung und Verstärkung der anti-viralen Antwort nach Interferon-Alpha Stimulation zur Folge haben. Des Weiteren wurde konstitutive, negative Rückkopplung durch nukleare Phosphatasen sowie induzierte negative Rückkopplung durch Neusynthese von SOCS Proteinen als Haupteinflüsse auf das kinetische Verhalten des Signalweges vorhergesagt. Die Prognose bezüglich IRF-9 Überexpression wurde daraufhin experimentell validiert. Ein Vergleich von Wildtyp-Zellen und IRF-9 Überexpressions-Zellen zeigte nach Interferon-Stimulation das von dem Modell vorhergesagte Verhalten für aktive Signaltransduktion-Proteine.

Des Weiteren wurde der Effekt auf der genetischen Ebene beobachtet, da ein entsprechendes Array-Experiment eine Hochregulation sowie eine Beschleunigung der Induktion von anti-viralen Genen, wie z.B. Mx1, zeigte. Demnach wurde die Überexpression von IRF-9 als Methode identifiziert, um den JAK/STAT Signalweg entscheidend zu verstärken.

Um die Mechanismen der individuellen Gen-Induktions-Muster zu erklären, die während des Array Experimentes beobachtet wurden, wurde eine bioinformatische Analyse durchgeführt. Die Analyse ergab, dass das Hub-Gen IRF1 in einem transkriptionellen Netzwerk involviert sein könnte, das die frühe und späte anti-virale Antwort kontrollieren könnte.

Um die Vorhersagen des Modells zu verbessern und die wesentlichen Reaktionen des Signalweges weiter einzugrenzen, was zu verbessertem Design von weiteren Experimenten führen könnte, wurde ein Zwei-Phasen Modellreduktionsansatz mit darauf folgenden Parameter-Schätzungen durchgeführt. Nach der ersten Reduktion wurde das Ursprungsmodell von 61 freien Parametern auf 33 freie Parameter reduziert, wobei das reduzierte Modell nach der entsprechenden Parameter-Schätzung die Fähigkeit beibehielt, sämtliche experimentelle Daten akkurat darzustellen. Die zweite Reduktion verkleinerte das Modell auf 22 freie Parameter, wobei dieses Modell weiterhin die experimentellen Daten gut darstellen konnte.

PUBLICATIONS

The following paper has been published from results of this thesis:

Maiwald, T., Schneider, A., Busch, H., Sahle, S., Gretz, N., Weiss, T. S., Kummer, U. and Klingmüller, U. (2010), Combining theoretical analysis and experimental data generation reveals IRF9 as a crucial factor for accelerating interferon α -induced early antiviral signalling. FEBS Journal, 277: 4741–4754. doi: 10.1111/j.1742-4658.2010.07880.x

Following publications are currently in progress:

Maiwald, T., Schneider, A., Surovtsova, I., Simus, N., Hüber, K., Klingmüller, U., Kummer, U. „Two-phase reduction of an interferon alpha signalling model utilizing time-scale-separation“

Schneider, A., Waldow, K., Maiwald, T., Busch, H., Kummer, U., Klingmüller, U. „Combining theoretical analysis and experimental data generation reveals transcriptional mechanisms underlying early and late anti-viral responses stimulated by interferon alpha“

INTRODUCTION

INTERFERON SUBTYPES

Interferons (IFNs) belong to the group of secreted cytokines and are named after their ability to interfere with viral activity. They allow communication between cells in the situation of a pathogenic threat to the organism. All known IFN subtypes bind to one of three receptor complexes and are therefore divided into three receptor-specific subgroups: Type I IFNs (discovered in 1957, (Isaacs et al. 1957)) including interferon α and β which play a pivotal role in the direct response to viral infections in most cell types. They bind to the IFN- α receptor (IFNAR). Following the receptor binding, the JAK/STAT signalling pathway gets activated, which is described in detail below. The class of type II IFNs consists of IFN- γ only, which binds to the IFN- γ receptor (IFNGR). Contrary to type I IFNs, IFN- γ is not secreted as a direct response to viral infection but exclusively by immune cells, e.g. T cells and natural killer cells, reasoning its alternative name “immune interferon” (Randall et al. 2008). IFN- γ stimulation of cells leads to the activation of another JAK/STAT signalling pathway by phosphorylation of STAT1 homodimers (Figure 1). These homodimers are then able to bind specific GAS-sites directly and induce the transcription of specific anti-viral genes. Three subtypes of IFN- λ have been recently classified as type III IFNs as they signal through a receptor complex consisting of IFNLR1 and IL10R2. Their function and associated signalling events are still barely understood but are under investigation (Onoguchi et al. 2007).

INTERFERON ALPHA SIGNALLING THROUGH JAK/STAT PATHWAY

IFN- α signalling through receptor complex IFNAR has been studied for the past two decades (Stark et al. 1998; Platanias 2005). The general mechanism of the underlying JAK/STAT signalling pathway has been well understood (Figure 1). Upon ligand binding, IFN receptor subunits IFNAR1 and IFNAR2 are able to bind as a heterodimer. This close approximation of the receptor subunits allows associated kinases JAK1 and TYK2 to initiate a phosphorylation cascade, first phosphorylating each other. Secondly, receptor binding sites are phosphorylated, which allow the signalling molecule STAT2 to bind to the receptor. During the next step of the cascade, STAT1 forms a heterodimer with receptor-associated STAT2. This dimer is stabilized through phosphorylation and released from the receptor. To form the transcriptionally active ISGF3 molecule, interferon regulatory factor 9 (IRF9/p48/ISGF3 γ) is bound to the phosphorylated STAT1/STAT2 heterodimer.

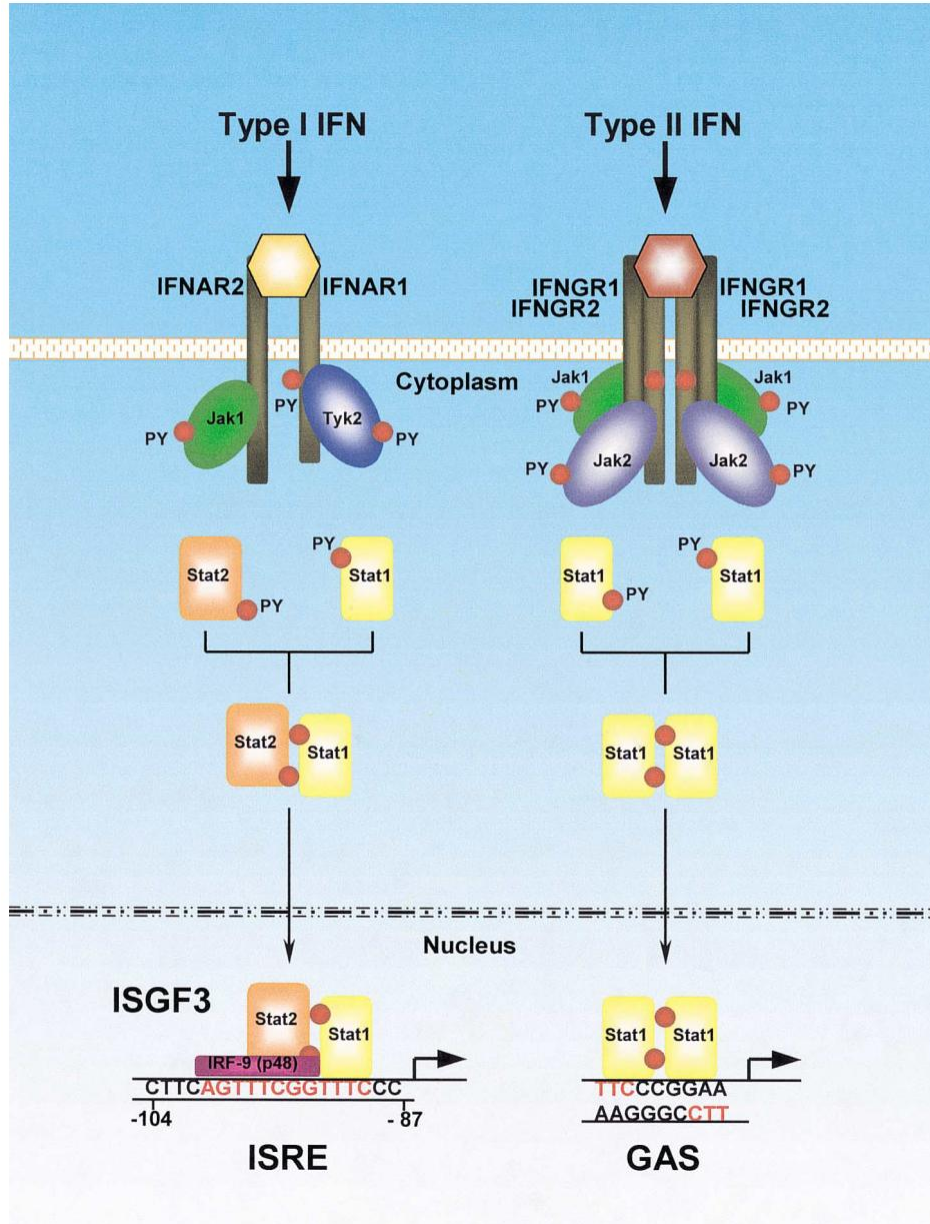


Figure 1 A schematic model of activation of the JAK–STAT pathway by IFN. Binding of IFNs to their receptors results in the activation of the cytoplasmic tyrosine kinases of the Janus kinase (JAK) family, JAK1 and TYK2 for IFN- α , and JAK1 and JAK2 for IFN- γ . Activated JAKs become phosphorylated and subsequently phosphorylate the receptor on specific tyrosine residues, which function as docking sites for the src-homology 2 (SH2) domain of STAT1 and STAT2. Tyrosine phosphorylation by JAKs results in heterodimerization of STAT1 and STAT2 or homodimerization of STAT1 and their nuclear translocation upon IFN- α or IFN- γ treatment, respectively. STAT1/STAT2 heterodimers bind to ISRE DNA sequence in the presence of IRF9 to form the ISGF3 complex whereas STAT1 homodimers bind to GAS directly. Kindly provided by Prof. A. E. Koromilas (Koromilas et al. 2001).

So far, IRF9 is known to be uniquely essential for IFN- α signalling, distinguishing it from other IFN signalling cascades, e.g. IFN- γ signalling. ISGF3 is then actively transported into the nucleus. In its trimeric form it is able to bind specific ISRE gene sites, the phosphorylated STAT1/STAT2 heterodimer on the other hand binds to non-specific binding sites (e.g. IFN- γ stimulated GAS-sites) (Li et al. 1996; Wesoly et al. 2007). Specific ISRE binding leads to a genetic response by transcription of anti-viral target genes, such as Mx1 or PKR (Der et al. 1998). The JAK/STAT signalling pathway is controlled through several feedback mechanisms. Constitutive negative feedback is performed through cytoplasmic and nuclear phosphatases (ten Hoeve et al. 2002). Dephosphorylation of the active STAT1/STAT2 complex leads to their separation into single proteins. They are then able to rebind the active receptor complex, leading to a phosphorylation cycle (Levy et al. 2002) (Figure 2). Dephosphorylation of the receptor is achieved by phosphatases SHP1 and SHP2 (You et al. 1999; Barua et al. 2007). The protein PIAS is responsible for another constitutive negative feedback. It is able to bind the ISGF3 complex and therefore specifically controlling the transcriptional activity of ISGF3 (O'Shea et al. 2004; Shuai 2006). Upon binding the DNA, ISGF3 induces gene transcription of additional feedback mechanisms. The dominant negative feedback being induced upon IFN stimulation is the SOCS protein. It is able to bind the active receptor complex and dephosphorylate the associated kinases or actively degrade the receptor complex, terminating the signalling cascade at the top level (Kile et al. 2002; Croker et al. 2008). Simultaneously, IFN- α signalling induces a positive feedback mechanism, namely the IRF9 transcription factor. Increasing the amount of IRF9 by overexpression or prestimulation of cells with IFN- γ or IL-6, results in a higher degree of transcription of interferon-stimulated genes (Bandyopadhyay et al. 1990; Levy et al. 1990; Tamada et al. 2002) and an augmented antiviral response (Leonard et al. 1997; Weihua et al. 2000). However, the specific impact of IRF9 on the dynamics of pathway activation remains to be identified.

MISSING LINKS & MEDICAL IMPACT

Many specifics such as dose-dependent influences of molecules on the kinetic behaviour of the signalling pathway have not been studied in detail. As time is the crucial factor to determine the success of an anti-viral response against a pathogen (Sarasin-Filipowicz et al. 2008), a precise understanding of the underlying kinetics is required for promising medical applications. Knowledge of kinetic-controlling molecule concentrations during various time-points and under diverse doses of stimuli, transcription factors and signalling mediators will provide us with significant information regarding screening applications or actual treatment. This holds especially true for feedback mechanisms, controlling the signalling pathway in a positive or negative way (Shuai et al. 2003). Surprisingly, studies analysing feedback influences in a time-resolved manner are still a rarity. IFN- α is used as a treatment of hepatitis C and B virus infection. However, the success of the treatment is highly patient-dependent (Manns et al. 2001). Differences between responders and non-responders are currently under investigation (Chen et al. 2005; Sarasin-Filipowicz et al. 2008), but have not been understood. Several other viral pathogens are known to induce genetic responses that hinder the IFN signalling pathway (Randall et al. 2008; Versteeg et al. 2010; Harman et al. 2011). Understanding viral interferences and their influence on the kinetic behaviour of the immune response is likely going to lead to new medical applications.

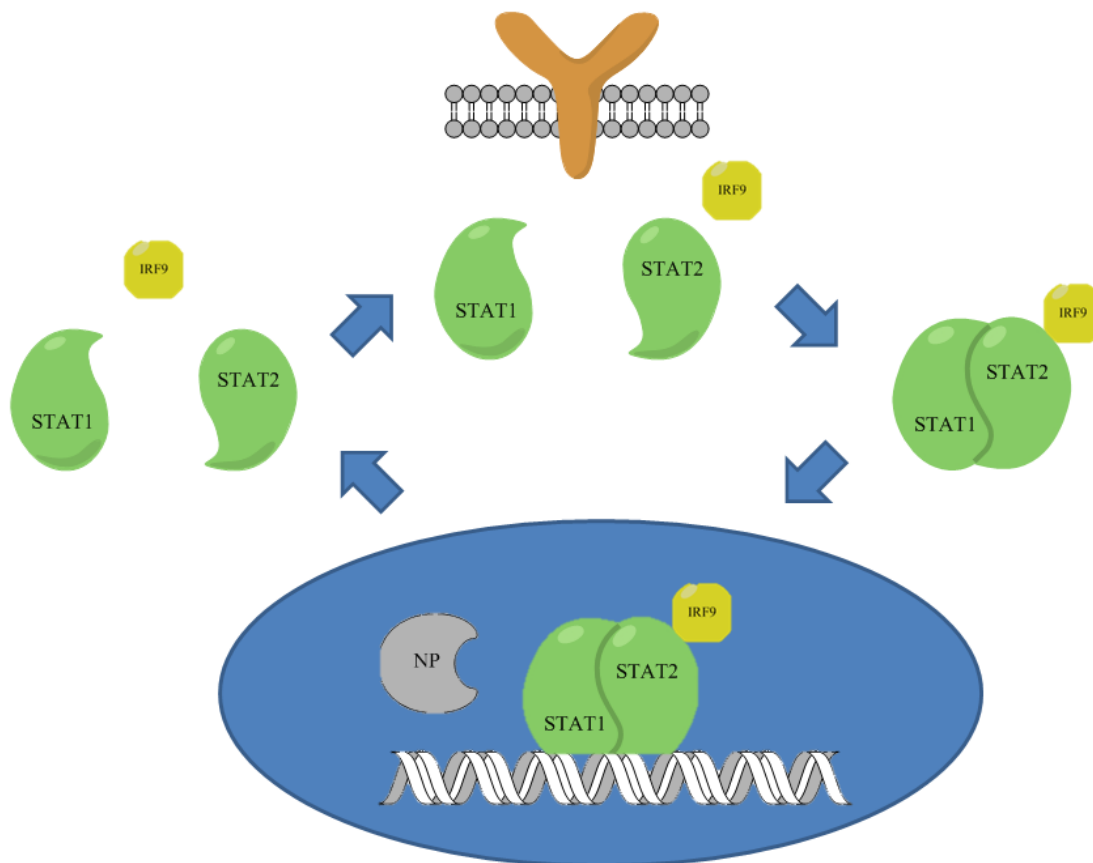


Figure 2 A schematic overview of the phosphorylation cycle. Upon receptor binding, STAT1, STAT2 and IRF9 become closely associated through phosphorylation (top/right). The active trimeric complex is then actively transported into the nucleus (right/bottom). Dephosphorylation through nuclear phosphatases leads to disassociation and the monomeric proteins are exported into the cytoplasm (bottom/left). If the receptor is still active, the exported subunits are able to rebind and reinitiate the phosphorylation cycle (left/top). NP: Nuclear phosphatase; Blue ellipse: Nucleus.

SYSTEMS BIOLOGY

As understanding of biological processes grows it is often surprising to witness the degree of complexity that is discovered. Underlying network structures are present on every level of biological life, e.g. on a population based level (Snijder et al. 2009), protein interactions in biological pathways (Schoeberl et al. 2002) or genetic networks controlled by differently transcribed transcription-factors (Zaslavsky et al. 2010). Looking at the interactivity of those networks, it is impossible to get a deeper insight without sophisticated computational tools that analyse and interpret known data (Kitano 2002a). Systems biology is focussing on the discovery of network structures and the according system dynamics (Kitano 2002b). Once a system is described or modelled in an appropriate way based on information provided by available experimental data, it is possible to use this model for predictions about the system. These predictions can be used to identify key experiments, which are then able to improve the quality of the model (Figure 3). Given that the required amounts of experimental data are available, a model is not only able to describe single pathways but also cross-talks, i.e. how sub-network influence each other in a time-resolved manner (Aldridge et al. 2009). Exemplary for future implications of utilizing systems biology are demonstrated by the concept of P4 medical treatment introduced by Hood et al. (Hood et al. 2011).

Looking at signalling pathways, systems biology has already been used to successfully deepen our insights into biological processes. In one example, modelling of the EGF signalling cascade has shown that not ligand concentration but initial velocity of receptor activation is the critical parameter for signal efficiency (Schoeberl et al. 2002). In another recent example, Epo signalling was investigated, uncovering that a rapid receptor turnover-rate is a decisive control mechanism required to cope with largely varying ligand concentrations (Becker et al. 2010). Apart from explaining biological processes in signalling pathways, theoretical systems biology has been used to propose new points of view for signal transduction, e.g. how a cell could interpret different messages from the same signal in a time-dependent resolution (Behar et al. 2010).

In summary, as our understanding of the complexity of biological processes rises, systems biology is a decisive tool to manage and learn from experimental data.

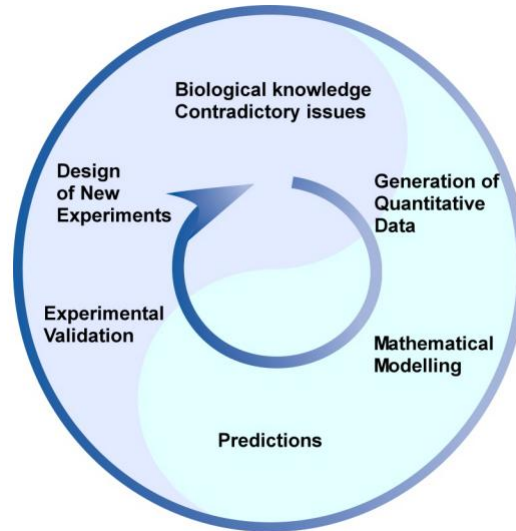


Figure 3 Hypothesis-driven research in systems biology. Systems biology approaches consist of an iterative process between experiments and modelling. Contradictory biological issues are answered in an iterative cycle of quantitative data generation, mathematical modelling, *in silico* predictions, experimental validation and design of new experiments. Adapted from (Kitano 2002b). Kindly provided by Annette Schneider.

MODELLING

Interferon signalling has been studied through computational modelling over the last decade. The majority of these studies have been focused on the IFN- γ signalling pathway (Yamada et al. 2003; Zi et al. 2005; Rateitschak et al. 2009). IFN- β signalling has been studied focussing on the pathway termination by constitutive negative feedback and the involvement of IFN- γ induced STAT1 homodimers (Smieja et al. 2008). As mentioned before, the difference between type I IFNs and type II IFNs is given by their signalling through different receptor complexes. IFN- γ induced signalling leads to the formation of phosphorylated STAT1 homodimers. The active STAT1/STAT1 homodimer is then able to bind IFN- γ specific GAS-sites (Figure 1) (Randall et al. 2008). Consequently, feedback mechanisms based upon the dephosphorylation of signalling mediators and receptors, e.g. nuclear phosphatases and induction of SOCS, respectively, apply

to both IFN signalling pathways. In the case of IFN- α however, the involvement of an additional transcription factor which is required for specific genetic response and in particular constitutes a positive feedback loop has a significant impact on the kinetic behaviour of the signalling cascade (Randall et al. 2008; Schoggins et al. 2011). Therefore, insights gained by studying the IFN- γ signalling pathway or kinetics controlled by phosphorylated STAT1 homodimers cannot be transferred to IFN- α signalling induced gene transcription.

AIM OF THE STUDY

In this study, a modelling approach has been performed to identify key molecules of the IFN- α pathway (Maiwald et al. 2010). The model combines known characteristics of the JAK/STAT signalling pathway, parameter values of similar modelling approaches from literature and experimental data. The aim of the modelling approach is to reproduce experimental measurements reliably and expand upon this knowledge to suggest hypotheses which can be experimentally verified. A main feature of the model is given by the comprehensive involvement of constitutive and induced feedback mechanisms. It is revealed through model simulation and experimental verification that overexpression of IRF9 leads to an augmented integrated response as well as an acceleration of IFN- α signalling. This alteration is directly affecting the genetic level, as experimental measurements show augmented and accelerated induction of most IFN- α 's target genes.

Furthermore, the model was improved using various approaches for model reduction and parameter estimation. First, the model was reduced using a sensitivity-driven method. Following up, a parameter estimation approach utilizing the profile likelihood method (Raue et al. 2009) based upon various experimental measurements was performed to improve the accuracy of the kinetic behaviour presented by the model. Results from the parameter estimation allowed the application of a time-scale separation based model reduction (Surovtsova et al. 2009).

RESULTS

MODELLING OF THE IFN ALPHA SIGNALLING PATHWAY

To examine the IFN- α signalling pathway and in particular the kinetic behaviour of its key components, a novel IFN- α signalling model was developed (Figure 4, Table 1). The model focuses on a comprehensive involvement of all known feedback mechanisms and unique traits of the IFN- α signalling pathway. This includes the requirement of the trimeric complex ISGF3 consisting of STAT1, STAT2 and IRF9 for specific gene induction, shuttling kinetics of key molecules and constitutive and induced feedbacks. Specifically, the model includes constitutive negative regulations by general phosphatases and PIAS as well as constitutive degradation of receptor, IRF9 and mRNA. Receptor dephosphorylation by SHP-2 was represented by a constant kinetic parameter, since changes in SHP-2 concentration were assumed to be negligible during the measured time-scale. Furthermore, the negative feedback loop of ISGF3-mediated SOCS induction was incorporated. As a positive feedback mechanism IRF9 synthesis was included since its IFN dependent expression was experimentally observed within the relevant time frame (Figure 5). Furthermore, certain behaviours of pathway components were based upon literature evidence: (i) IRF9 is constitutively bound to STAT2 in its unphosphorylated form (Martinez-Moczygema et al. 1997), (ii) unphosphorylated STAT1 and STAT2 molecules constantly shuttle between nucleus and cytoplasm, while nuclear import of STAT2 is increased by IRF9 binding (Banninger et al. 2004) and (iii) unbound IRF9 is mainly localised in the nucleus (Lau et al. 2000) (for a detailed description see [model description](#)). The rate law interpretation of the model is assumed to be deterministic.

MODEL DESCRIPTION

The developed model consists of 38 species and 41 kinetic reactions (Table 1). Nearly all reactions are assumed to be mass action kinetics. Michelis-Menten kinetic requires a prerequisite condition to be satisfied: Substrate concentration must exceed enzyme concentration significantly. As this is usually not the case in signal transduction pathways, Michelis-Menten kinetic is neglected in the analysis (Yamada et al. 2003). Two reaction subtypes are excluded from this scheme: Nuclear/cytoplasmic shuttling and transcriptional activity. These reactions are influenced by modifiers which are independent of the reaction itself, namely compartment sizes, occupied DNA-binding sites and cytoplasmic mRNA, respectively. Therefore, those reactions required the introduction of individual kinetic functions. As a prerequisite, free kinases (JAK and TYK) bind free receptor subunits (IFNAR 1 and IFNAR 2) (Table 1, reaction 1 / 2). Resulting receptor-subunits with attached kinases trimerise with a free IFN molecule into an active receptor complex (IFNAR dimer) (Table 1, Reaction 3). This active complex is able to bind free cytoplasmic STAT2 and subsequent free cytoplasmic STAT1 (Table 1, reaction 5-7). The next reaction describes STAT phosphorylation and leads to an unbinding of the phosphorylated STAT1/STAT2 heterodimer from the active receptor (Table 1, reaction 8). Heterodimers can either bind cytoplasmic IRF9 to build the ISGF-3 complex (Table 1, reaction 9) or get transported actively into the nucleus (Table 1, reaction 11), where they are able to bind nuclear IRF9 (Table 1, reaction 12). Cytoplasmic ISGF-3 is transported actively into the nucleus as well (Table 1, reaction 10). Once in the nucleus, ISGF-3 is able to bind to free DNA binding sites (Table 1, reaction 13). Their DNA-binding induces transcriptional activity (Table 1, reaction 14 / 15), leading to production of more IRF9 as a positive feedback and SOCS as a negative feedback (Table 1, reaction 16 / 17). SOCS is able to block and degrade active receptors through binding the catalytic cleft of a kinase using the kinase inhibitory region (KIR) and receptor ubiquitination, respectively, therefore terminating additional STAT phosphorylation (Crocker et al. 2008) (Table 1, reaction 18). Furthermore, several constitutive negative feedbacks play a role in the model. Cytoplasmic and nuclear

phosphatases dephosphorylate both ISGF-3 and phosphorylated STAT heterodimers, in the cytoplasm and the nucleus, respectively, leading to the complex dissociating into its monomeric subunits STAT1, STAT2 and IRF9 (Table 1, reaction 23-30). DNA binding protects ISGF3 of nuclear phosphatases (Meyer et al. 2003) which is taken into account through adjusted kinetic parameters (Table 1, reaction 31 / 32). Other feedbacks like PIAS, specifically inhibiting nuclear ISGF-3 (Chung et al. 1997) (Table 1, reaction 33), constitutive receptor, IRF9 and mRNA degradation (Table 1, reaction 18 / 20-22 / 34) and receptor-level phosphatases (SHP2, (Frearson et al. 1997)) (Table 1, reaction 19) were also included. Their presence ensures no loss of information about possible interplays and dependencies between different species regarding the kinetic behaviour of the model that would be neglected by a minimalistic approach. Further reactions include: IRF9 is constitutively bound to unphosphorylated STAT2 in the unstimulated system in both compartments (Table 1, reaction 37 / 38) (Reich et al. 2006). Constant shuttling of unphosphorylated STAT1 and STAT2 between cytoplasm and nucleus occurs (Table 1, reaction 35 / 36), while nuclear import of STAT2 is increased by IRF9 binding (Table 1, reaction 39) (Reich et al. 2006). Free IRF9 shuttles between cytoplasm and nucleus, but it is mainly localised in the nucleus (Table 1, reaction 40) (Lau et al. 2000).

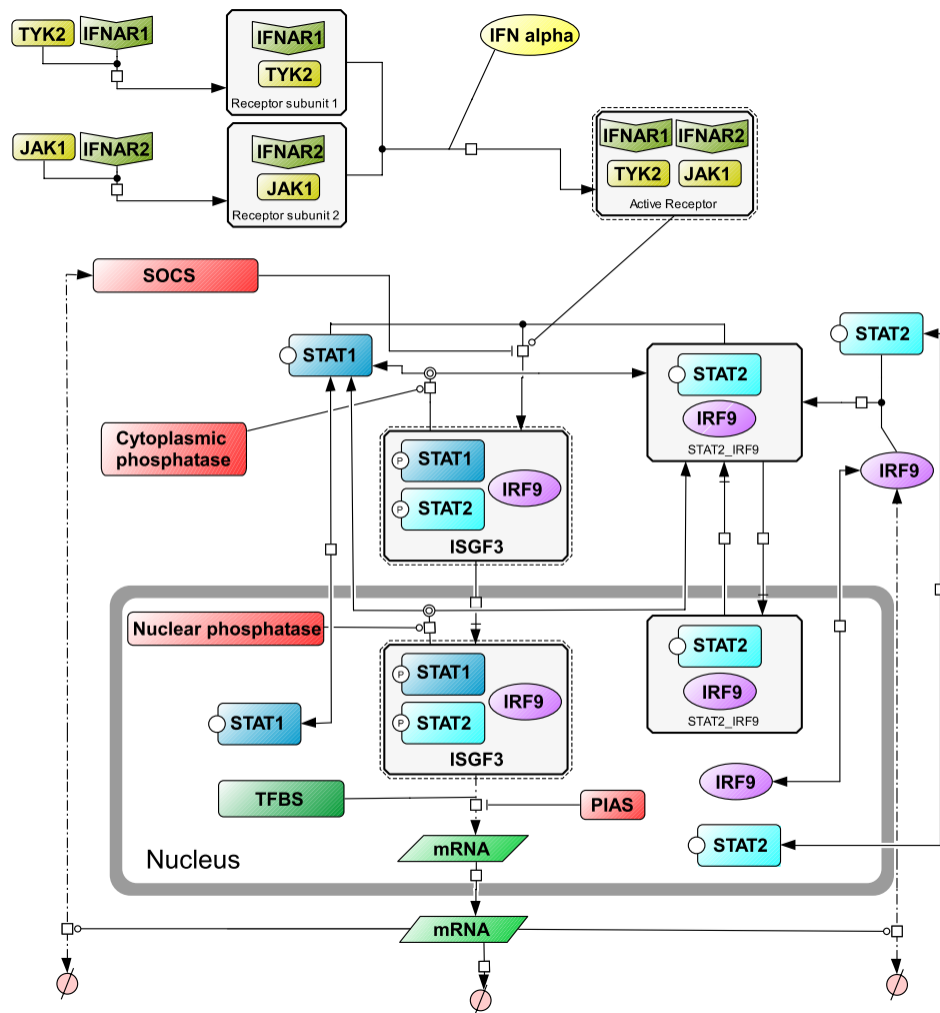


Figure 4 Schematic overview of the full IFN- α signalling model. A simplified view of the model architecture is shown with the activation of STAT proteins summarised in one reaction and omitting receptor endocytosis, constitutive IRF9 degradation and nuclear translocation of phosphorylated STAT1/STAT2 heterodimers. For details see Table 1. Lines with empty circles: reaction catalysis; lines with perpendicular bars: reaction inhibition; dotted lines: transcription; TFBS: transcription factor binding site. The scheme was generated using CellDesigner (Kitano et al. 2005).

Results - Model description

Nr.	Reaction	Kinetic rate law
1	Receptor IFNAR 1 + TYK = Receptor Tyk Complex	$k1*s1*s2 - k2*p1$
2	Receptor IFNAR 2 + JAK = Receptor Jak Complex	$k3*s1*s2 - k4*p1$
3	Receptor Jak Complex + Receptor Tyk Complex + IFN_free = IFNAR dimer	$k5*s1*s2*s3 - k6*p1$
4	IFNAR dimer -> Active Receptor Complex	$k7*s1$
5	STAT2c_IRF9 + Active Receptor Complex -> Active Receptor Complex_STAT2c + IRF9c	$k8*s1*s2$
6	STAT2c + Active Receptor Complex = Active Receptor Complex_STAT2c	$k9*s1*s2 - k10*p1$
7	STAT1c + Active Receptor Complex_STAT2c = Active Receptor Complex_STAT2c_STAT1c	$k11*s1*s2 - k12*p1$
8	Active Receptor Complex_STAT2c_STAT1c -> Active Receptor Complex + STAT1c*_STAT2c*	$k13*s1$
9	IRF9c + STAT1c*_STAT2c* = ISGF-3c	$k14*s1*s2 - k15*p1$
10	ISGF-3c = ISGF-3n	$k16*s1 - k17*p1$ (com partment change)
11	STAT1c*_STAT2c* = STAT1n*_STAT2n*	$k18*s1 - k19*p1$ (com partment change)
12	STAT1n*_STAT2n* + IRF9n = ISGF-3n	$k20*s1*s2 - k21*p1$
13	ISGF-3n + Free transcription factor binding site(TFBS) = Occupied TFBS	$k22*s1*s2 - k23*p1$
14	\emptyset -> mRNA _n	$k24*modifier$ (Occupied TFBS)
15	mRNA _n = mRNA _c	$k25*s1 - k26*p1$ (com partment change)
16	\emptyset = IRF9c	$k27 + k28*modifier - k29*p1$ (mRNA _c)
17	\emptyset = SOCS	$k30*modifier - k31*p1$ (mRNA _c)
18	Active Receptor Complex -> Receptor IFNAR1 + Receptor IFNAR2 + JAK + TYK	$k32*s1 + k33*s1*modifier$ (SOCS)
19	Active Receptor Complex -> IFNAR dimer	$k34*s1$
20	IRF9n -> \emptyset	$k35*s1$
21	STAT2c_IRF9 -> STAT2c	$k36*s1$
22	STAT2n_IRF9 -> STAT2n	$k37*s1$
23	ISGF-3c + Cytoplasmic phosphatase(CP) = ISGF-3c_CP	$k38*s1*s2 - k39*p1$
24	ISGF-3c_CP -> STAT1c + STAT2c + CP + IRF9c	$k40*s1$
25	STAT1c*_STAT2c* + CP = STAT1c*_STAT2c*_CP	$k41*s1*s2 - k42*p1$
26	STAT1c*_STAT2c*_CP -> STAT1c + STAT2c + CP	$k43*s1$
27	STAT1n*_STAT2n* + Nuclear phosphatase(NP) = STAT1n*_STAT2n*_NP	$k44*s1*s2 - k45*p1$
28	STAT1n*_STAT2n*_NP -> STAT1n + STAT2n + NP	$k46*s1$
29	ISGF-3n + NP = ISGF-3n_NP	$k47*s1*s2 - k48*p1$
30	ISGF-3n_NP -> STAT1n + STAT2n + NP + IRF9n	$k49*s1$
31	Occupied TFBS + NP = Occupied TFBS_NP	$k50*s1*s2 - k51*p1$
32	Occupied TFBS_NP -> STAT1n + STAT2n + IRF9n + Free TFBS + IRF9n	$k52*s1$
33	PIAS + ISGF-3n = PIAS_ISGF-3n	$k53*s1*s2 - k54*p1$
34	mRNA _c -> \emptyset	$k55*s1$
35	STAT1c = STAT1n	$k56*s1 - k57*p1$ (com partment change)
36	STAT2c = STAT2n	$k58*s1 - k59*p1$ (com partment change)
37	STAT2c + IRF9c = STAT2c_IRF9	$k60*s1*s2 - k61*p1$
38	STAT2n + IRF9n = STAT2n_IRF9	$k62*s1*s2 - k63*p1$
39	STAT2c_IRF9 = STAT2n_IRF9	$k64*s1 - k65*p1$ (com partment change)
40	IRF9c = IRF9n	$k66*s1 - k67*p1$ (com partment change)
41	IFN_influx -> IFN_free	$k68*s1$

Table 1 Overview of kinetic reactions and equations. Second column shows reaction formulas. “=” defines reversible reactions, “->” irreversible reactions, respectively. Third column displays according kinetics. Compartment changes are considered. Suffixes: c: cytoplasm, n: nucleus, “*”: phosphorylated. Kinetic rate laws: s: substrate, p: product according to their correspondent reactions

Results - Model description

Nr.	Source for reference value (if none = trained)		
1	k1 : 0.1	k2 : 0.05	Yamada et al. 2003, Zi et al. 2005
2	k3 : 0.1	k4 : 0.05	Yamada et al. 2004, Zi et al. 2005
3	k5 : 0.01	k6 : 0.01	Jaks et al. 2007, Gavutis et al. 2006, Yamada et al. 2003
4	k7 : 0.005		Yamada et al. 2003, Zi et al. 2005
5	k8 : 0.002		Smieja et al. 2008
6	k9 : 0.002	k10 : 4	Smieja et al. 2008
7	k11 : 0.002	k12 : 4	Yamada et al. 2003, Zi et al. 2005
8	k13 : 8		Smieja et al. 2008
9	k14 : 0.1	k15 : 0.1	
10	k16 : 0.015	k17 : 0	
11	k18 : 0.015	k19 : 0	Smieja et al. 2008
12	k20 : 0.01	k21 : 0.01	
13	k22 : 0.1	k23 : 0.1	
14	k24 : 0.000025		Smieja et al. 2008
15	k25 : 0.001	k26 : 0	Yamada et al. 2003
16	k27 : 0.005	k28 : 0.045	k29 : 0.0001
17	k30 : 0.045	k31 : 0.0005	Yamada et al. 2003, Zi et al. 2005
18	k32 : 0.0003	k33 : 0.000012	Yamada et al. 2003, Zi et al. 2005
19	k34 : 0.01		Yamada et al. 2003, Barua et al. 2007
20	k35 : 0.0001		
21	k36 : 0.0001		
22	k37 : 0.0001		
23	k38 : 0.001	k39 : 0.2	Yamada et al. 2003, Zi et al. 2005, Smieja et al. 2008
24	k40 : 0.003		Yamada et al. 2003, Zi et al. 2005, Smieja et al. 2008
25	k41 : 0.001	k42 : 0.2	Yamada et al. 2003, Zi et al. 2005, Smieja et al. 2008
26	k43 : 0.003		Yamada et al. 2003, Zi et al. 2005, Smieja et al. 2008
27	k44 : 0.01	k45 : 0.1	Yamada et al. 2003, Zi et al. 2005, Smieja et al. 2008
28	k46 : 0.1		Yamada et al. 2003, Zi et al. 2005, Smieja et al. 2008
29	k47 : 0.01	k48 : 0.1	Yamada et al. 2003, Zi et al. 2005, Smieja et al. 2008
30	k49 : 0.002		Yamada et al. 2003, Zi et al. 2005, Smieja et al. 2008
31	k50 : 0.0001	k51 : 0.1	
32	k52 : 0.1		
33	k53 : 0.1	k54 : 0.1	
34	k55 : 0.0005		
35	k56 : 0.00125	k57 : 0.01	Yamada et al. 2003, Zi et al. 2005, Smieja et al. 2008
36	k58 : 0.0000817	k59 : 0.0014	Smieja et al. 2008
37	k60 : 0.01	k61 : 0.01	
38	k62 : 0.01	k63 : 0.01	
39	k64 : 0.00125	k65 : 0.0014	
40	k66 : 0.02	k67 : 0.005	
41	k68 : 0.0009		

Table 2 Overview of kinetic parameters. According sources that were taken into account as reference values are shown in the last row (Yamada et al. 2003; Zi et al. 2005; Gavutis et al. 2006; Barua et al. 2007; Jaks et al. 2007; Smieja et al. 2008). Reactions are numbered according to Table 1.

For model calibration kinetic parameters were taken from literature (Table 2) or trained against experimental data (Figure 5) with all kinetic parameters being estimated within a physiologically meaningful range, i.e. within six orders of magnitude. The initial concentrations of STAT1, STAT2, JAK1, TYK2 and IRF9 were experimentally determined (Figure 6, Table 3). Measurements of phosphorylation levels of STAT molecules showed that approximately 30% of the total amount of STAT molecules were phosphorylated after IFN alpha stimulation. This is in accordance with literature (Vinkemeier 2004). Finally, the major signalling peak is assumed to occur between 20 and 60 minutes after IFN alpha stimulation. As mentioned above, the model includes all known feedback mechanisms of the IFN- α signalling pathway. This is necessary to analyse their specific impact in a time-dependend perspective. Consequently, this leads to a comprehensive model which represents an underdetermined system due to the number of unknown kinetic parameters in comparison to the amount of available data points. However the established model is consistent with the experimental data (Figure 5) and permits qualitative predictions.

Results - Model description

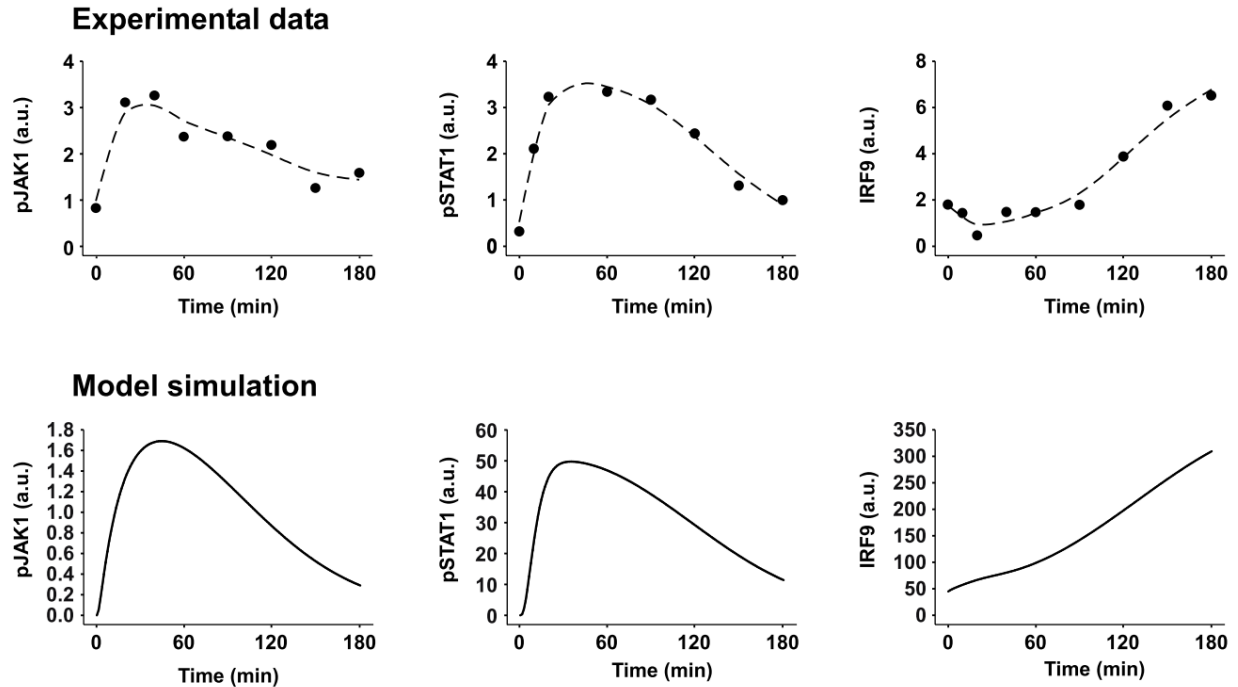


Figure 5 Dynamic behaviour of IFN alpha signalling. Activation of pJAK1, pSTAT1 and IRF9 measured by quantitative immunoblotting after stimulating Huh7.5 cells with 500 U/ml IFN alpha. A representative plot is shown, the experiment was repeated at least three times (see Figure 8A for additional data). The error bars represent a technical relative error of 18%, derived from multiple measurements. Experiments were performed by Annette Schneider. Filled circles: experimental data; dashed lines: smoothing splines; a.u.: arbitrary units. Model simulation (line) for pJAK1, pSTAT1 and IRF9 performed with COPASI (Hoops et al. 2006). The simulations are within the range of data reproducibility.

Species	Initial Concentration
IFNAR1	1000
IFNAR2	1000
JAK	26
TYK	13
IFN	6.5
STAT1	1500
STAT2	500
IRF9	45 (900)
CP	20
NP	40
PIAS	10
TFBS	500

Table 3 Initial concentrations of model species [nmol/l]. Concentrations of STAT1 and phosphatases are from Yamada et al. (Yamada et al. 2003). Measured concentrations (JAK1, TYK2, STAT1, STAT2, IRF9) were transformed from molecules per cell to nmol/l by using STAT1 concentration as reference. Concentrations for receptors (IFNAR1, IFNAR2) were assumed to be non-limiting and therefore set to a high amount.

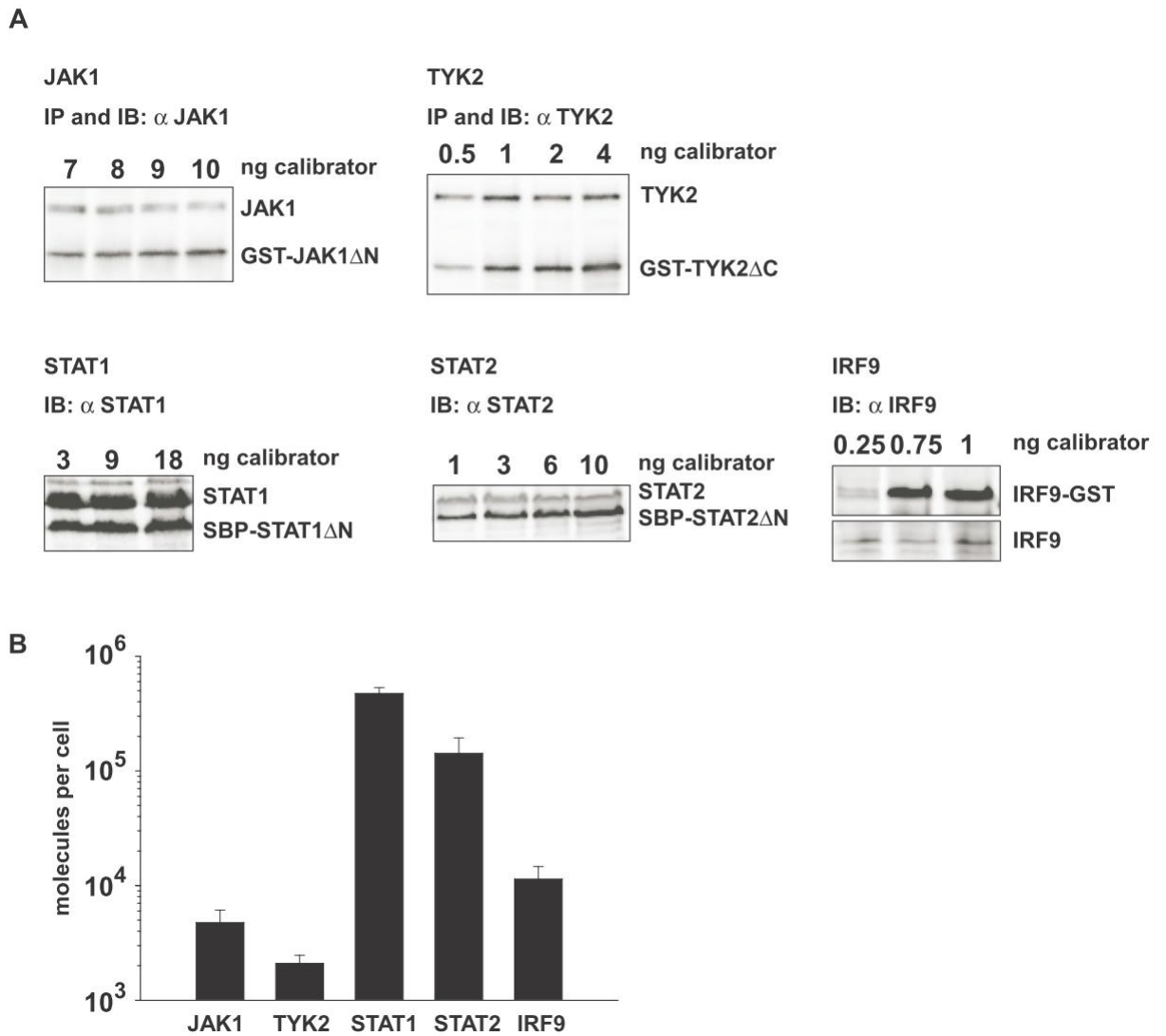


Figure 6 Protein quantification of key pathway components. (A) Dilution series of recombinant calibrator proteins were added to cell lysates of Huh7.5 cells and the relative amount of the respective protein was determined using quantitative immunoblotting in at least triplicates. For JAK1 and TYK2, an immunoprecipitation was performed prior to immunoblotting. (B) The absolute amount of endogenous proteins per cell was calculated using the calibrator dilution series as reference, accounting for the molecular weight of the recombinant and the endogenous proteins as well as the number of lysed cells. Molecules/cell: JAK1: 5000; TYK2: 2000; STAT1: 474000; STAT2: 142000; IRF9: 11000. Experiments were performed by Annette Schneider

HYPOTHESIS: IRF9 OVEREXPRESSION AMPLIFIES SIGNALLING KINETICS

To systematically identify key components responsible for the speed and extent of the IFN- α signalling, a local sensitivity analysis was performed (Figure 7A). As an input, the initial protein concentrations of the pathway components were varied. Two kinetic behaviours were chosen as an output: (i) The peak time and (ii) the area under the curve of the ISGF-3 concentration in the nucleus. These system quantities were selected as the concentration of ISGF-3 molecules which is bound to the DNA is crucial for the transcriptional activation of an antiviral response. Therefore, peak time represents the speed of signalling, whereas the integrated response corresponds to the amount of signalling that occurs.

In contrast to other systems, for which control is widely distributed (Hornberg et al. 2005), only few molecules controlled the systems behaviour of IFN alpha signalling. Nuclear phosphatases show a prominent negative effect on the integrated response while accelerating the occurrence of the signalling peak, which is in line with previous theoretical studies (Heinrich et al. 2002). Higher doses of free interferon lead to an increased signal amplitude but barely affect the peak time and signal duration, which could be confirmed experimentally (Figure 8B). Focusing on signal mediators STAT1 and STAT2, they present a positive control over the integrated response as well as a minor deceleration of the signalling peak.

Results - Hypothesis: IRF9 overexpression amplifies signalling kinetics

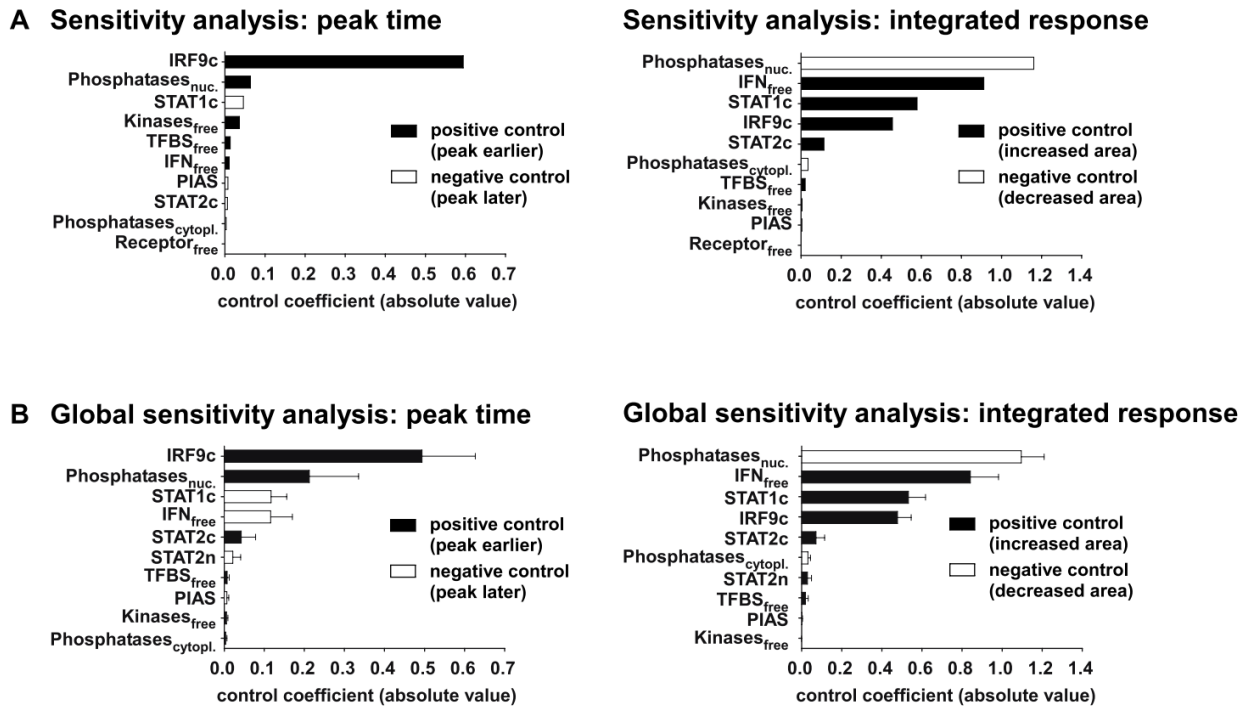


Figure 7 Sensitivity analysis for peak time and integrated response. Initial concentrations of all players were varied to calculate their control coefficient on the kinetic behaviour of the system. NP/CP: nuclear/cytoplasmic phosphatases. (A) Sensitivity analysis using the original parameter set. (B) Global sensitivity analysis using an array of 998 parameter sets.

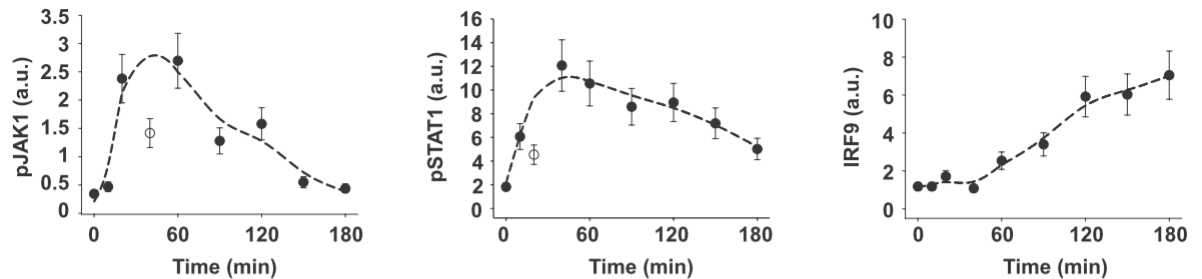
The only component that implements a major positive control simultaneously over speed and amount of signalling is transcription factor IRF9.

To ascertain that the results derived by the sensitivity analysis were not restricted to the original parameter set, the same approach was repeated using diverse parameter sets. For this purpose, random search implemented in Copasi's optimization task was used to vary all model parameters between +/- 50% of their original value. As fitting constraints, the resulting kinetic behaviours had to reproduce the experimental data (Figure 5). Through this process, 998 different parameter sets matching the given criteria were obtained. Further analysis of these data sets showed that the kinetic parameters could vary quite substantively and still reproduce the experimental data. Therefore, given the system being underdetermined, it is important to examine parameter sensitivities not only on a single point in parameter space, but rather use a more global approach. The

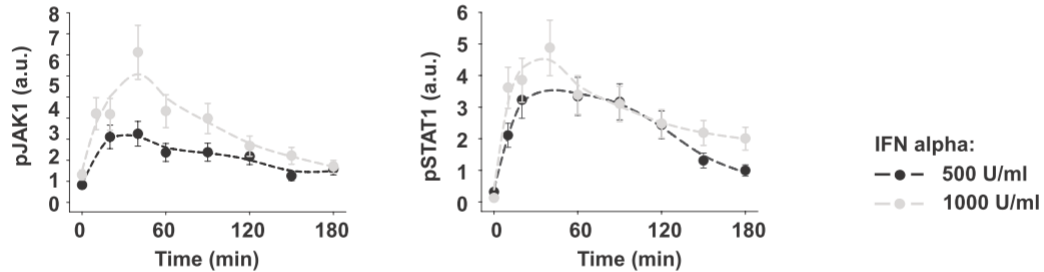
obtained parameter sets were used for a global sensitivity analysis. As shown in Figure 7B, the most sensitive component in both analyses was IRF9, supporting its central role. The role of free IFN differed between both approaches regarding the time of the signalling peak: Whereas the locale approach showed a minor positive influence (Figure 7A), the global analysis revealed an increased negative control coefficient for most parameter sets (Figure 7B). However, as in the experimental data the peak time for different interferon doses was comparable (Figure 8B), it was reasonable to retain the original parameter set for further analysis. In conclusion, major sensitivities were conserved throughout the parameter space, confirming that IRF9 has an important impact on the kinetic behaviour of the system independent of specific parameter sets.

Sensitivity analyses describe small changes for each given parameter to examine an impact on the kinetic behaviour of the system. To prove that large variations of IRF9 concentrations behaved accordingly, additional model simulations were performed. Indeed, a major increase in IRF9 levels accelerated signal transduction from the cytoplasm to the nucleus, resulting in a greater amount of active ISGF3 in the nucleus at earlier time points (Figure 9A). Furthermore, the model predicted a steeper signalling decline after the peak for elevated IRF9 levels. To test if this effect was a result of upregulated transcription of negative inhibitors (SOCS proteins), we removed SOCS1-induction *in silico*. Without this negative feedback, signal termination was attenuated in the IRF9 overexpressing cells, while in the wildtype cells IRF9 de novo-synthesis accounted for enhanced signalling during the analysed time frame (Figure 10A).

A Huh7.5 cells



B Huh7.5 cells



C Primary human hepatocytes

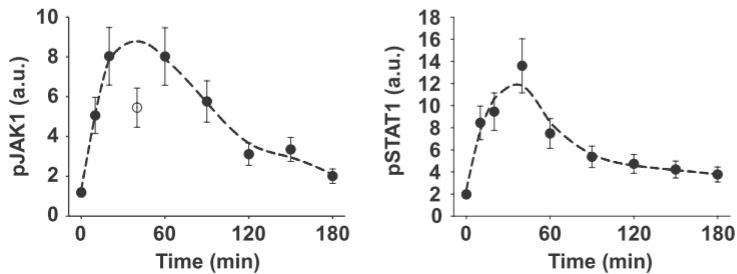
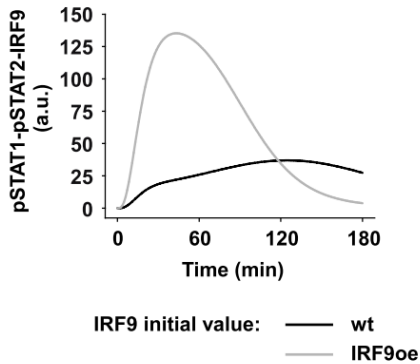
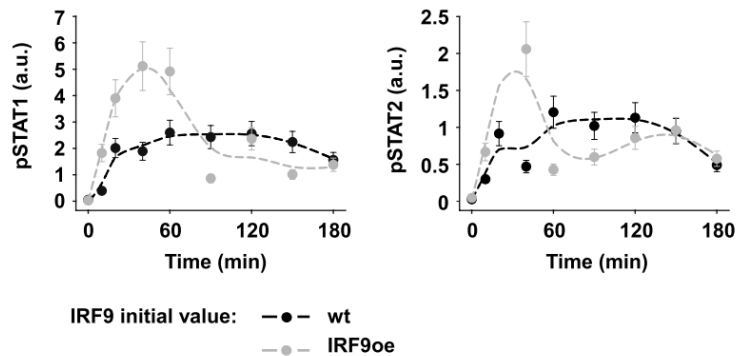


Figure 8 Additional data describing the dynamics of IFN alpha signalling in Huh7.5 cells and primary human hepatocytes. The error bars represent a technical relative error of 18%, derived from multiple measurements. Dashed lines: smoothing splines. **(A)** Activation of key components measured by quantitative immunoblotting after stimulating Huh7.5 cells with 500 U/ml IFN alpha. Open circles represent data points that were treated as outliers. **(B)** Activation of key components measured by quantitative immunoblotting after stimulating the cells with 500 U/ml or 1000 U/ml IFN alpha. **(C)** Activation of key components measured by quantitative immunoblotting after stimulating primary human hepatocytes with 500 U/ml IFN alpha. Experiments were performed by Annette Schneider.

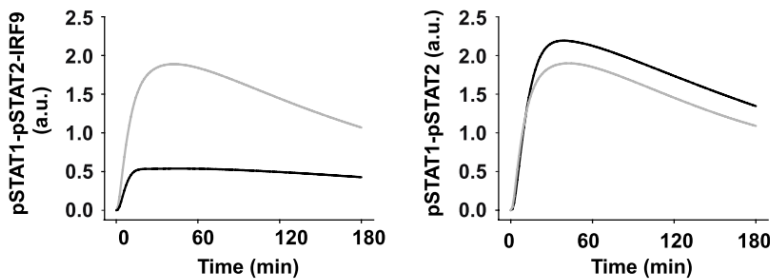
A Model prediction



B Experimental validation



C Increased nuclear import



Phosphatase protection

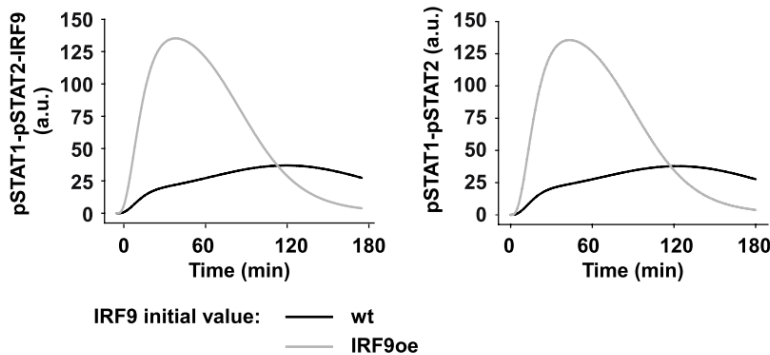
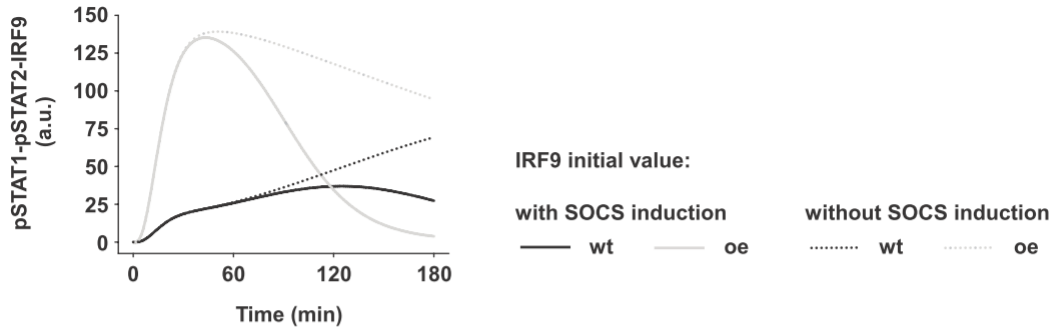


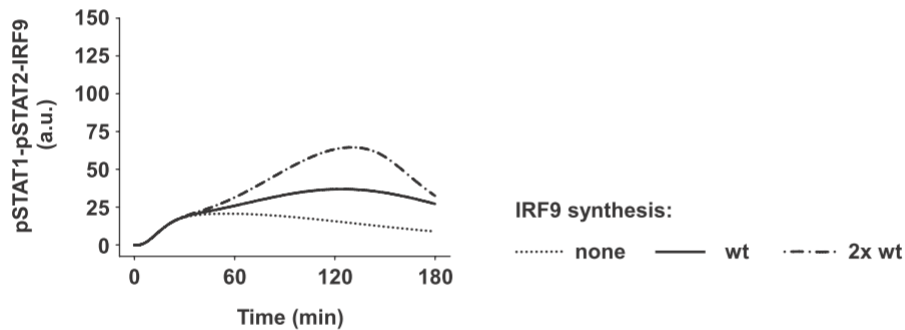
Figure 9 IRF9 controls dynamics of IFN alpha signalling. (A) Model prediction of IFN alpha-dependent ISGF3 (pSTAT1-pSTAT2-IRF9) accumulation in the nucleus, which is equivalent to the predicted kinetics of pSTAT1/pSTAT2. Simulations (lines) were performed for wild type cells (wt) and for cells with 32 fold IRF9 overexpression (IRF9oe). (B) Experimental validation of the model prediction. Wild type Huh7.5 cells (wt) or Huh7.5 cells stably overexpressing IRF9 32 fold (IRF9oe) were stimulated with 500 U/ml IFN alpha and phosphorylation of nuclear STAT proteins was measured by quantitative immunoblotting. The error bars represent a technical relative error of 18%, derived from multiple measurements. Filled circles: experimental data; dashed lines: smoothing splines; a.u.: arbitrary units. Experiments were performed by Annette Schneider. (C) In silico analysis of two potential mechanisms for the effect of IRF9. Simulation of DNA bound ISGF3 and pSTAT1-pSTAT2 heterodimers in the nucleus, in case of IRF9 leading to increased nuclear import of pSTAT1-pSTAT2 and in case of IRF9 protecting from phosphatase degradation.

Results - Hypothesis: IRF9 overexpression amplifies signalling kinetics

A Effect of SOCS synthesis



B Effect of IRF9 induction



C mRNA production

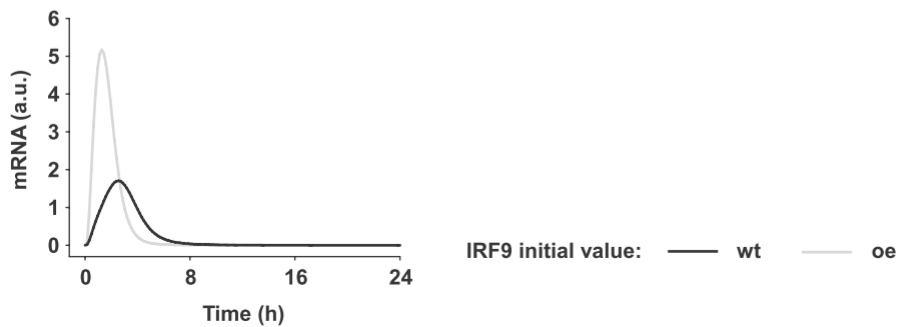


Figure 10 In silico analysis of changes in feedback control and their effects on kinetic behaviours of different components. (A) Concentration of occupied TFBS in wild-type (wt) and IRF9-overexpression (oe) simulation with and without SOCS synthesis. (B) Concentration of ISGF3 occupied TFBS in wild-type simulation with no IRF9 synthesis, regular IRF9 synthesis and enhanced IRF9 synthesis. (C) Concentration of total mRNA levels in simulations of wild-type and IRF9-overexpression.

To experimentally validate the model predictions, IRF9 was stably overexpressed in Huh7.5 cells by lentiviral transduction*. The phosphorylation kinetics of nuclear STAT1 and STAT2 in response to stimulation with 500 U/ml IFN alpha was determined by quantitative immunoblotting (Figure 9B)*. In line with the model analysis, IRF9-overexpressing cells showed a higher and earlier activation peak in the nucleus as well as a steeper peak decline compared to wild type cells. To determine if different IRF9 induction rates could have a similar effect, we varied the parameter for IRF9 synthesis *in silico*. Indeed, a more rapid IRF9 synthesis resulted in enhanced IFN alpha signalling, while eliminating the positive feedback dampened the response (Figure 10B).

In principle, the effects of IRF9 could be achieved by two mechanisms. First, IRF9 could decelerate dephosphorylation of activated STAT1/2, since phosphorylated STAT1/2 complexes can only bind specifically to ISRE sites in combination with IRF9 and DNA-bound STAT proteins are protected from nuclear phosphatase activity (Meyer et al. 2003). This mechanism was implemented in the model. As a potential alternative mechanism, nuclear import of phosphorylated STAT1/2 could be increased upon interacting with IRF9. This is based on the observation that IRF9 possesses a strong constitutive nuclear localisation signal (NLS) recognized by a variety of importins, whereas the NLS of phosphorylated STAT1/2 heterodimers is only recognized by importin α -5 (Reich 2007). Therefore the complex harbouring both types of NLS could have an increased chance to interact with a matching importin resulting in enhanced nuclear translocation kinetics.

To dissect the impact of both effects we performed model simulations. *In silico* analysis indicated that increased IRF9-dependent nuclear import kinetics, while neglecting IRF9 mediated phosphatase protection, could not represent the experimental data. On the contrary, our model describing the observed dynamics solely with IRF9 dependent phosphatase protection of DNA-bound ISGF3 was necessary and sufficient to reproduce the observed kinetic data (Figure 9C).

Hence, our analysis identified IRF9 as crucial for both rapid and efficient IFN alpha-mediated signal transduction and suggests prolongation of DNA-binding of ISGF3 as the underlying mechanism.

PROVING FURTHER IMPACT OF IRF9 CONCENTRATION THROUGH EXPERIMENTAL MEASUREMENTS

To test whether the accelerated and enhanced nuclear presence of phosphorylated STAT1/2 proteins upon IRF9 overexpression resulted in altered gene activation kinetics, expression kinetics of IFN alpha-stimulated genes were analysed by quantitative real time PCR*. RNA levels of the antiviral genes PKR (Balachandran et al. 2000) and ISG56 (Terenzi et al. 2008) as well as the negative inhibitors SOCS1 (Alexander 2002) and USP18 were determined at different time points for up to 24 hours. USP18 was discovered as a protease cleaving the IFN-induced, ubiquitin-like modifier ISG15 from its target proteins (Malakhov et al. 2002), but recently was also reported to block phosphorylation of JAK1 (Malakhova et al. 2006).

The examined genes were strongly induced by IFN alpha (Figure 11A). Interestingly, each gene analysed displayed different expression kinetics, suggesting gene-specific, promoter-dependent regulation mechanisms. SOCS1 exhibited a very fast induction followed by a rapid repression. USP18, on the other hand, displayed an increased expression for up to 24 hours. Similar to USP18, the antiviral genes ISG56 and PKR showed a prolonged upregulation. Interestingly, for all genes investigated induction of gene expression was faster when IRF9 levels were elevated, which was consistent with the general mRNA induction predicted by the model (Figure 10C). For ISG56, SOCS1 and USP18 a high IRF9 level also resulted in an increased peak amplitude, whereas for PKR the peak amplitude was unaltered. The integrated response was larger for each of the four genes, with a more pronounced difference during the first 4 hours (Figure 11A).

Results - Proving further impact of IRF9 concentration through experimental measurements

To confirm that the observed effect was not restricted to the tested genes, we investigated the global induction of IFN alpha stimulated genes by a time-resolved microarray (Figure 11B/C). For data analysis, genes were selected that showed a more than one fold relative expression in both wildtype and IRF9 overexpressing cells upon stimulation with interferon alpha. A gene ontology analysis using DAVID (Huang et al. 2008) showed that those resulting 284 genes are related to immune and virus response as well as antigen processing and presentation, as expected (Table 4). Gene expression time series were characterized regarding difference in mean fold expression and difference in temporal regulation (see [Materials and Methods](#) for details).

There was an overall positive correlation between the level of gene expression and the expression kinetics: genes that were stronger upregulated in the IRF9 overexpressing cells were also induced earlier. Remarkably, this was true for the majority of the genes in IRF9 overexpressing cells compared to wildtype cells (160 out of 257). One exception was IRF9 itself, as it could not be induced much beyond the already high expression level in overexpressing cells. Taken together, these data demonstrate that an elevated amount of IRF9 not only results in higher levels of transcription, but also in accelerated IFN alpha target gene expression.

Results - Proving further impact of IRF9 concentration through experimental measurements

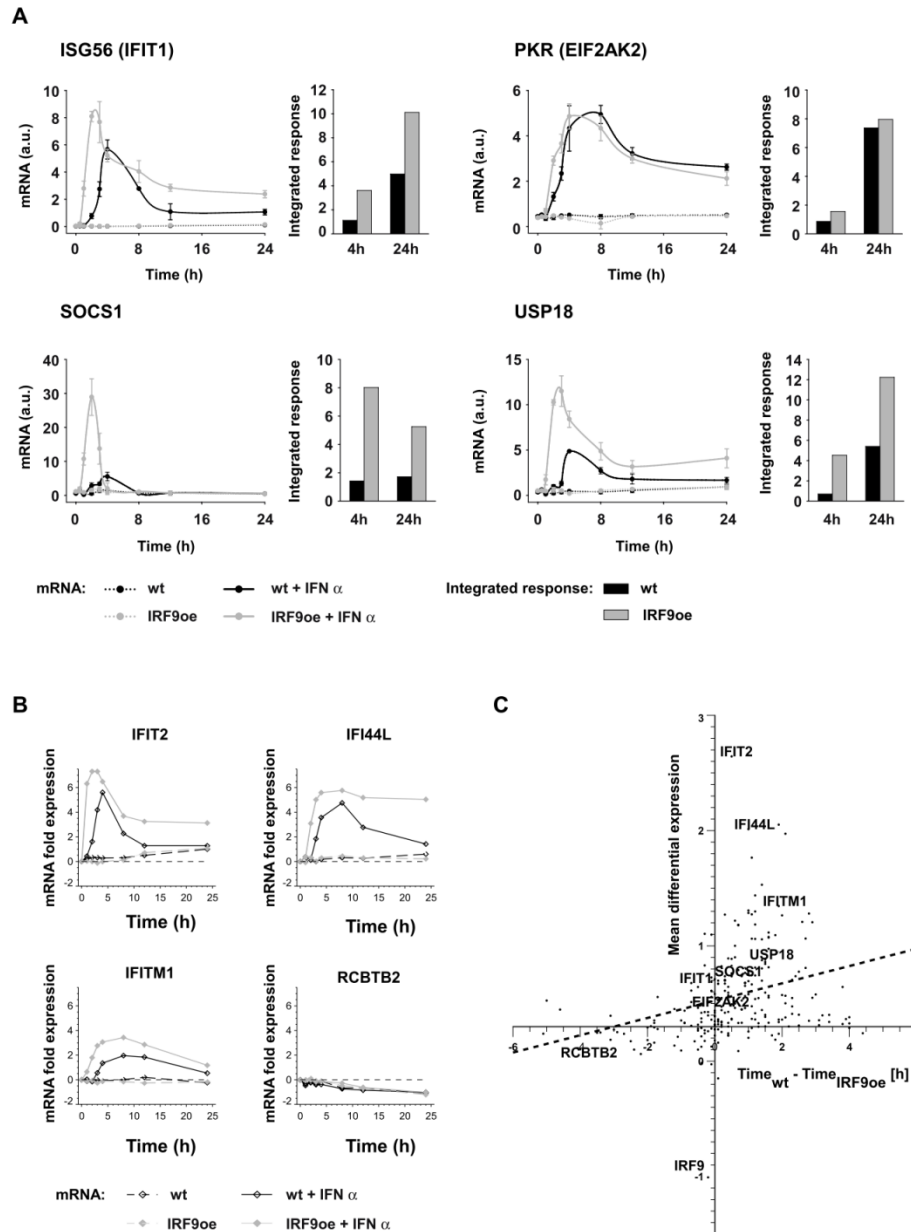


Figure 11 IRF9 controls dynamics of IFN alpha induced gene expression. Huh7.5 wildtype cells stably transduced with an empty vector (wt) or IRF9-overexpressing cells (IRF9oe) were stimulated with 500 U/ml IFN alpha and RNA was extracted in biological triplicates at the indicated time points. **(A)** Quantitative real time PCR analysis of four exemplary genes. For each gene, the integrated response up to an early (4 h) and a late (24 h) time point was calculated. Experiments were performed by Annette Schneider. **(B - C)** Time resolved microarray analysis performed with one replicate per time point. Experiment was performed by Annette Schneider and Norbert Gretz. Analysis was performed by Hauke Busch. **(B)** Kinetics of representative genes in Huh7.5 wildtype cells stably transduced with an empty vector (wt) or IRF9-overexpressing cells (IRF9oe) **(C)** Scatter plot depicting the difference in gene induction time and mean fold expression in control or IRF9 overexpressing cells. Positive values designate accelerated and augmented gene expression in IRF9oe cells. The plotted genes are regulated more than one fold in either wildtype or IRF9 overexpressing cells and have less than six hours difference in gene induction time (257 genes). Additionally, SOCS1 and IRF9 are included. There is a clear trend for faster and augmented gene expression in the IRF9 overexpressing cells, demonstrated by the linear regression (slope: 0.08; p-value: 0.00006). Genes from A and B are highlighted in bold.

Results - Proving further impact of IRF9 concentration through experimental measurements

Annotation Cluster	Enrichment Score	Count	P-Value
Annotation Cluster 1 Enrichment Score: 13.16			
immune response		43	6.4E-16
immune system process		50	8.1E-15
response to stimulus		93	6.5E-11
Annotation Cluster 2 Enrichment Score: 9.86			
response to virus		17	2.9E-12
response to biotic stimulus		26	2.2E-10
multi-organism process		34	5.6E-10
response to other organism		22	9.9E-10
Annotation Cluster 3 Enrichment Score: 4.46			
response to chemical stimulus		42	5.9E-7
defense response		25	7.2E-6
response to stress		46	2.0E-5
response to external stimulus		30	4.0E-5
response to wounding		20	2.1E-4
inflammatory response		13	2.4E-3
Annotation Cluster 4 Enrichment Score: 4.44			
antigen processing and presentation		13	2.0E-9
antigen processing and presentation of peptide antigen via MHC class I		7	8.4E-8
antigen processing and presentation of peptide antigen		7	2.2E-6
MHC class I protein complex		6	3.4E-5
antigen processing and presentation of exogenous antigen		4	9.2E-4
MHC protein complex		6	1.1E-3
antigen processing and presentation of exogenous peptide antigen		3	1.0E-2
MHC class I receptor activity		3	2.2E-2
Annotation Cluster 5 Enrichment Score: 4.01			
antigen processing and presentation of peptide antigen via MHC class I		7	8.4E-8
antigen processing and presentation of peptide antigen		7	2.2E-6
antigen processing and presentation of endogenous peptide antigen via MHC class I		3	2.9E-3
antigen processing and presentation of endogenous peptide antigen		3	2.9E-3
antigen processing and presentation of endogenous antigen		3	5.3E-3
Annotation Cluster 6 Enrichment Score: 3.43			
response to nutrient		11	3.2E-5
response to vitamin A		6	3.1E-4
response to vitamin		7	3.5E-4
response to nutrient levels		11	5.3E-4
response to retinoic acid		5	1.2E-3
response to extracellular stimulus		11	1.2E-3
Annotation Cluster 7 Enrichment Score: 3.2			
positive regulation of cell communication		16	7.5E-5
positive regulation of signal transduction		15	8.5E-5
regulation of cell communication		30	3.6E-4
positive regulation of I-kappaB kinase/NF-kappaB cascade		8	4.7E-4
regulation of I-kappaB kinase/NF-kappaB cascade		8	8.4E-4
positive regulation of protein kinase cascade		9	2.7E-3
regulation of protein kinase cascade		11	3.0E-3
regulation of signal transduction		24	3.4E-3
Annotation Cluster 8 Enrichment Score: 2.41			
regulation of response to stimulus		22	3.0E-6
positive regulation of response to stimulus		13	1.5E-4
regulation of response to stress		14	1.5E-4
regulation of immune system process		16	4.1E-4
regulation of defense response		9	1.0E-3
regulation of immune response		11	1.5E-3
positive regulation of immune system process		10	7.1E-3
innate immune response		7	1.4E-2
regulation of innate immune response		4	4.2E-2
Annotation Cluster 9 Enrichment Score: 2.13			
microsome		11	1.6E-3
vesicular fraction		11	1.9E-3
cell fraction		25	1.3E-2
insoluble fraction		20	2.1E-2
membrane fraction		19	2.8E-2

Table 4 GO analysis of the 284 genes with at least 1-fold upregulation in both wildtype and IRF9 overexpressing cells. Annotation clusters with an overall enrichment score >2 were regarded as significant. The Count column denotes the number of genes found in the respective GO category. The P-Value column denotes the EASE score, the modified Fisher exact p-value for the respective GO category. Analysis has been performed by Hauke Busch.

UNDERSTANDING THE DIVERSE GENETIC RESPONSE THROUGH A BIOINFORMATICS APPROACH

As gene expression kinetics showed a diverse behaviour upon stimulation with IFN- α (Figure 11A), further investigations were required. In theory, several mechanisms are able to explain the observed pattern, especially regarding the difference between early response (0-8 hours after stimulation) and late response (8-24 hours after stimulation). These theories involve:

- Gene expression networks, where the early response triggers the expression of a transcription factor that activates a secondary, late response (Zaslavsky et al. 2010)
- Control through posttranscriptional modifications, e.g. microRNA (Anderson 2010)
- Autocrine stimulation by expression of a potent ligand, that is secreted into the extracellular environment (Shvartsman et al. 2002)
- Differences in the stability of individual mRNAs (Guhaniyogi et al. 2001; Hao et al. 2009)

Although these theories might work together in synergy, narrowing the possible explanations for the observed behaviour was the aim for further analyses. Specifically, finding potential target proteins for additional experimental measurements was the main focus. Therefore, a bioinformatics approach was chosen using the STRING database (Szklarczyk et al. 2011). The STRING database utilizes text-mining algorithms, protein-interaction databases and documented experiments to visualize a protein-interaction network for given proteins of interest. Using key proteins of the JAK/STAT signalling pathway as an input the network structure was predicted to resemble a cascade (Figure 12). In detail, highlighted through the red rectangle on the left is ISGF-3, the signalling mediator of the JAK/STAT pathway. A green and yellow connection between STAT1 and IRF1 represents activation and expression, which is followed by an activation connection from IRF1 to DDX58 (RIG-I). This route shows the only transcriptionally active path from ISGF-3 towards known IFN- α induced targets on the right side of the cascade, i.e. MX1 and ISG15. The central node in this

predicted network structure is represented by IRF1. IRF1 is a well-studied hub-gene, i.e. it is known to regulate a variety of specific responses. For instance, IRF1 is involved in the anti-viral response as a positive feedback (Kalvakolanu V 2003; Pitha 2011), it is able to bind to a consensus sequences that are very similar to the ISRE, namely IRF-E and induces several DNA damage response genes (Frontini et al. 2009). It has recently been identified to induce a specific gene pattern, partly overlapping with the IFN- α induced response but independent of the JAK/STAT signalling pathway (Stirnweiss et al. 2010).

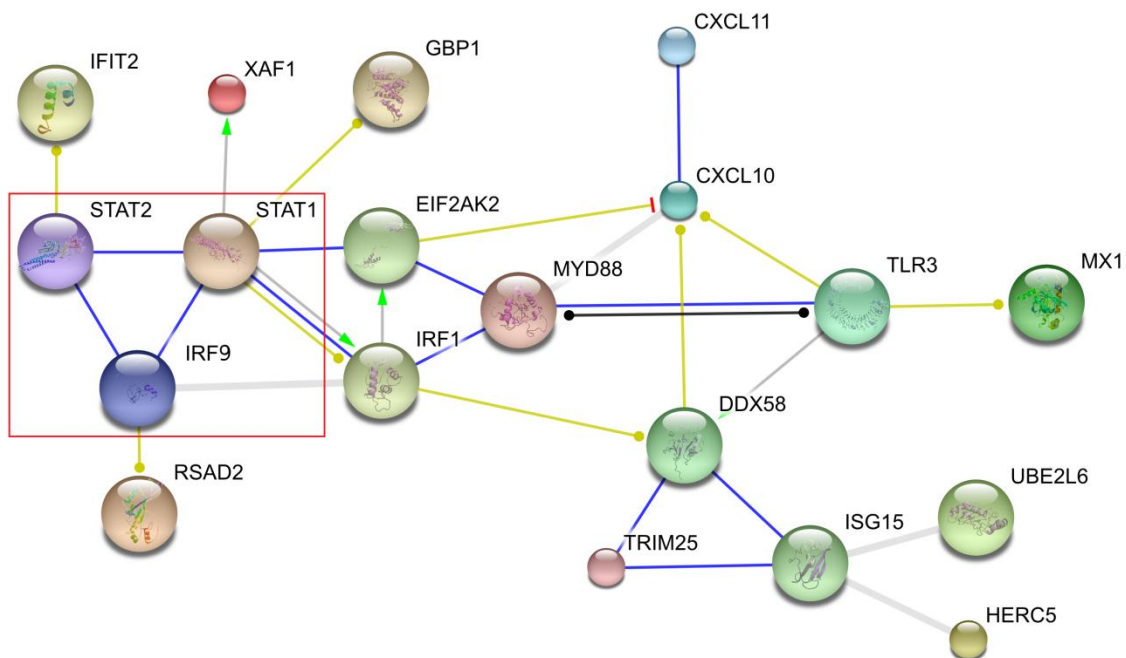


Figure 12 Visualization of the STAT1/STAT2/IRF9 induced protein network using STRING database. Connecting lines between balls represent a known interaction between both proteins. Connections were predicted using the highest possible confidence score. Red rectangle: ISGF3 complex, grey line: unspecified interaction, blue line: Binding, yellow line with yellow dot: Expression, yellow line with red bar: Inhibition, black line: Reaction, green line: Activation.

MODEL REDUCTION AND PARAMETER ESTIMATION

To get a deeper understanding of the IFN- α signalling pathway, eliminating assumptions, such as parameters gathered from literature which might not be valid in our experimental setup, was the next major goal of the project. Therefore, experimental data of different JAK/STAT related proteins under various conditions were obtained through time-course measurements performed by Annette Schneider (Figure 13). All measurements were performed after cells have been treated with a standard IFN- α stimulus (500 U/ml) unless stated otherwise. Specifically, these measurements included:

- Concentration of phosphorylated STAT molecules in the nucleus for wildtype and IRF9 overexpression cells (Figure 13, first row)
- Concentration of phosphorylated receptor complexes, phosphorylated STAT molecules in the cytoplasm and IRF9 in the nucleus for wildtype cells (Figure 13, second row)
- Concentration of phosphorylated STAT molecules in cytoplasm and nucleus for standard and increased dosage of IFN- α stimulus (increased: 1000 U/ml) (Figure 13, third row)
- Concentration of phosphorylated STAT molecules in cytoplasm and nucleus for wildtype and IRF9 overexpression cells with the addition of an actinomycin D treatment, inhibiting transcriptional activity (Figure 13, fourth and fifth row)
- Concentration of SOCS mRNA for wildtype and IRF9 overexpression cells (Figure 13, sixth row, first and second column)
- Concentration of SOCS protein for wildtype and IRF9 overexpression cells (Figure 13, sixth row, third and fourth column)

Results - Model reduction and parameter estimation

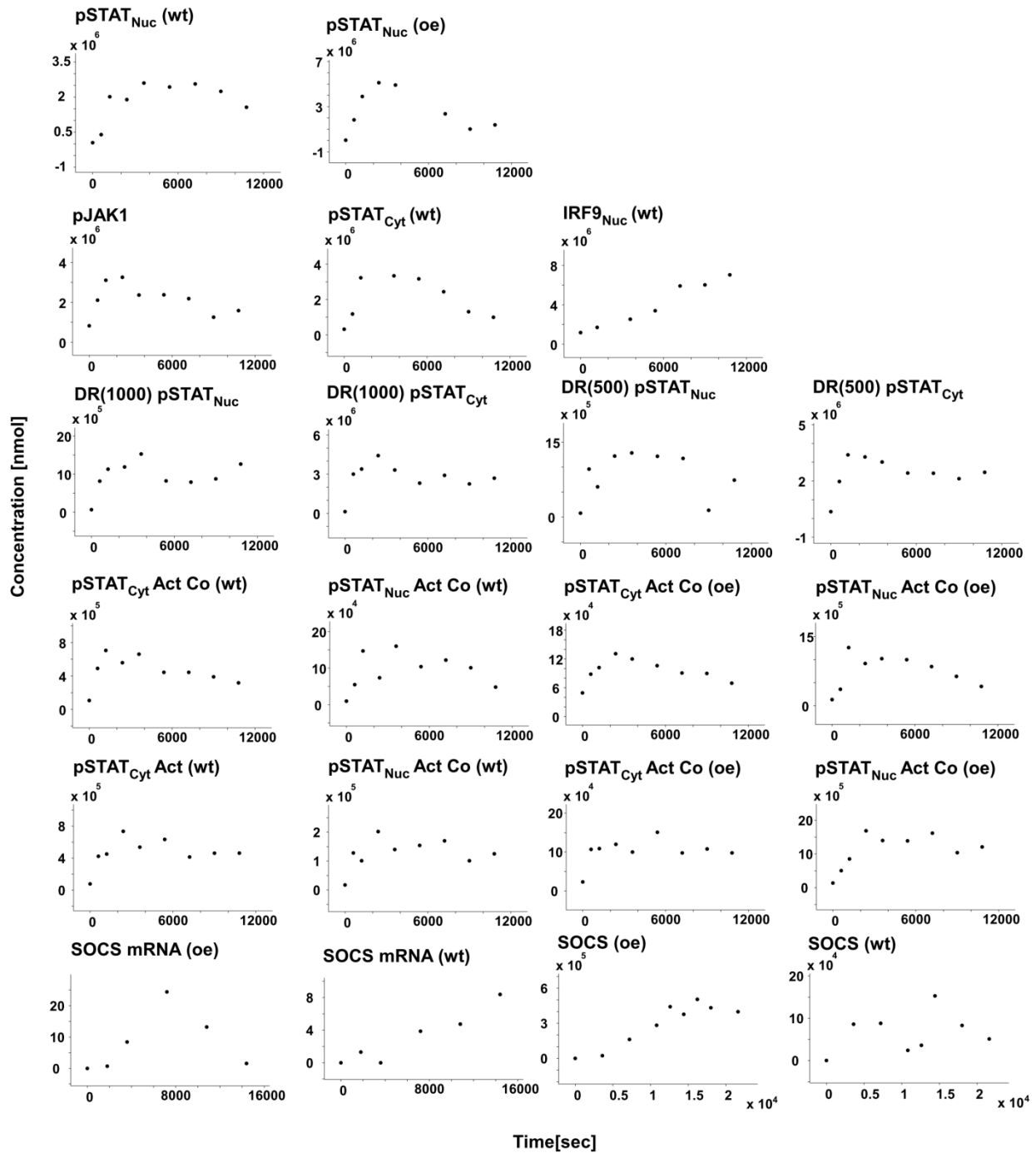


Figure 13 Data points of experimental measurements X-axis describes the time in seconds, y-axis the concentration of the according experimental measurement. Plot titles indicate the performed experiment. Individual data points are shown as dots.

As a result, measurements provided approximately 180 data points which were appropriate for parameter calibration through a parameter estimation approach. Parameter estimation describes the method of estimating kinetic parameters by comparing given data points against the kinetic behaviour of corresponding concentrations in the model. The comparison is scored which allows the usage of various algorithms in an attempt to optimize the problem by changing the value of the input (free parameters) to get to the lowest possible score (accuracy of the fit) (Chen et al. 2010). However, as the model described earlier contains 61 free parameters, the ratio between free parameters and available data points suggests that many diverse parameter sets are able to reproduce the data. Therefore, using the original model for a parameter estimation approach will lead to non-conclusive results.

A statistical test for finding the most suitable model for a given set of data points is defined as the ratio between the lowest fitting score and the number of degrees of freedom in a regression (Jaquaman et al. 2006). In this test, the lowest value of interest defines the most suitable model.

$$1) \text{ degrees of freedom} = \text{datapoints} - \text{free parameters}$$

$$2) \text{ value of interest} = \frac{\text{fitting score}}{\text{degrees of freedom}}$$

Concluding, the most suitable model combines a low fitting score with the lowest possible amount of free parameters. To improve the number of degrees of freedom, a model reduction approach was chosen. The aim of a model reduction approach is to decrease the number of kinetic parameters of a model by maintaining the ability to fit given data points accurately.

As a first step, 183 locale parameter fitting approaches were performed for the original model using Potterswheel (Maiwald et al. 2008). In detail, all given model parameters are randomly disturbed around their initial value. Then, they are locally optimized leading into the closest minimum in the surrounding parameter space. The resulting locale fits were sorted score-wise and the top 25% were selected for further analysis (Figure 14). Using the selected parameter sets, averages, standard deviations and coefficients of variation of according parameters were calculated (Table 5). Coefficients of variation varied immensely

between model parameters. Most parameters with minor impact on the kinetic behaviour of the system belonged to side-reactions of the pathway and constitutive feedbacks while induced feedbacks such as transcription of IRF9 and SOCS and reactions that were responsible for transducing the signal were displayed in the low coefficient of variation sector. Consequently, for the current model structure, parameters with a low coefficient of variation have to be conserved within a certain threshold to produce an accurate fit of the experimental data while parameters with high coefficients of variation do not have a profound impact on the kinetic behaviour of protein concentrations of interest. As a first approach to reduce the model, parameters were sorted according to their coefficient of variation and additional local fitting calculations were performed where only sub-groups of low coefficient of variation parameters were given as an input. An exemplary case is illustrated in Table 5 where the cut-off between free and fixed parameters is illustrated by a blue line. All other parameters were fixed to their original value. By testing several amounts of free parameters in that way, fitting approaches showed that selecting the 33 parameters with the lowest standard deviation as free parameters while fixing the other 28 parameters (which are presumed to be removable) was the lowest amount of free parameters that could still fit the data points sufficiently.

Following this result, the original model was reduced by mainly simplifying reactions that were fixed during the previous approach aiming towards a model consisting of 33 parameters. Therefore, model reactions were modified or deleted accordingly (For a detailed description see [Materials and Methods](#)) (Figure 15, Table 6 and Table 7).

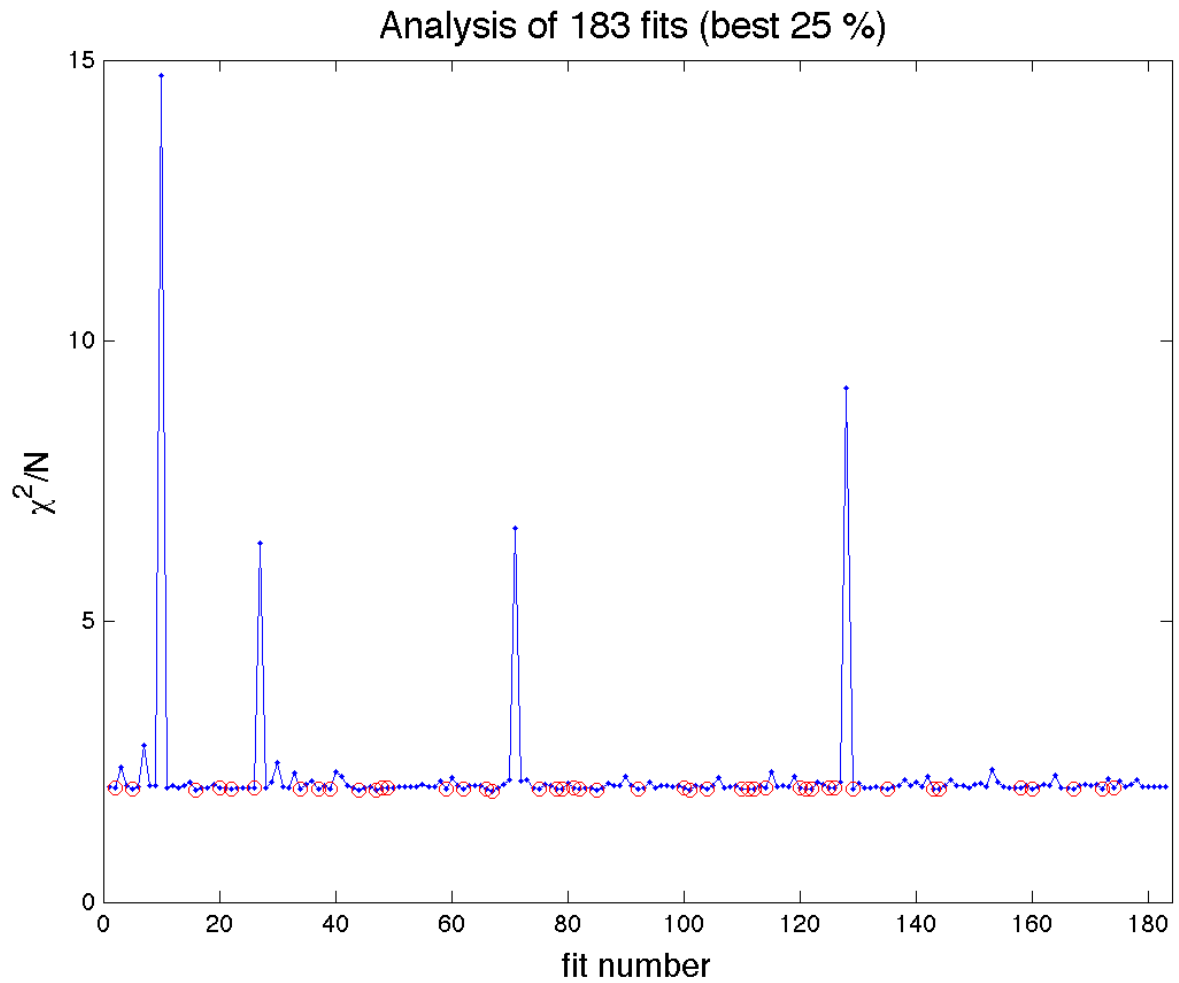


Figure 14 Set of 183 locale fits and their corresponding fitting score. Each dot along the blue line depicts one locale fitting approach starting from randomly disturbed initial parameter values. X-axis shows the fit number, y-axis presents the fitting score divided by the number of free parameters N . The best 25% of the fitting approaches have been selected for further analysis and marked by a red circle. Figure produced using Potterswheel (Maiwald et al. 2008).

Results - Model reduction and parameter estimation

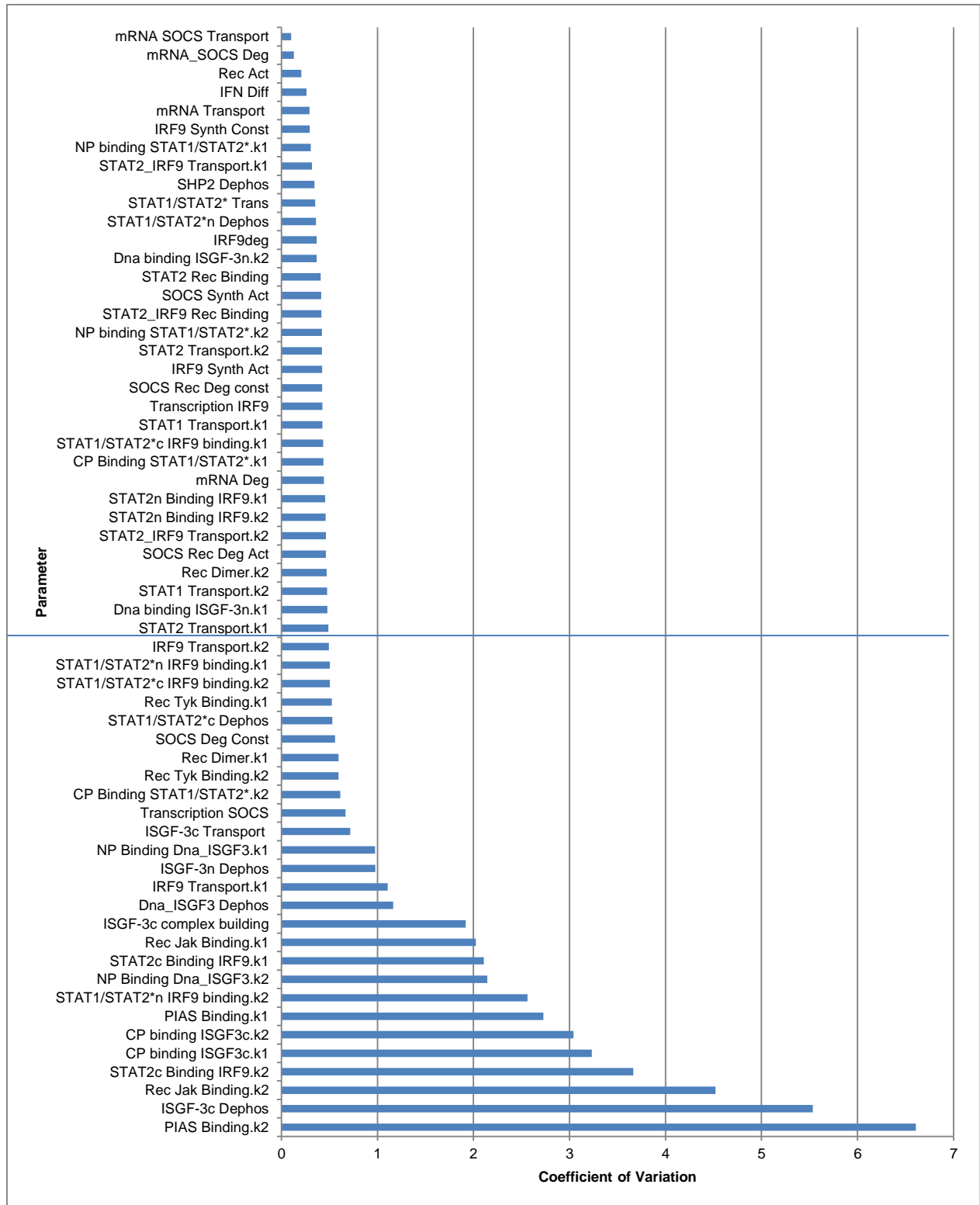


Table 5 Coefficients of Variation for all parameters in the full model. Selected local fitting approaches shown in Figure 14 were analysed and their according coefficient of variation was calculated. X-Axis shows coefficient of variation, y-axis the parameter name. Table is sorted according to coefficient of variation. Blue line presents the cut-off for further analysis. The 33 parameters above the cut-off were used as free input parameters while the parameters below the blue line were fixed.

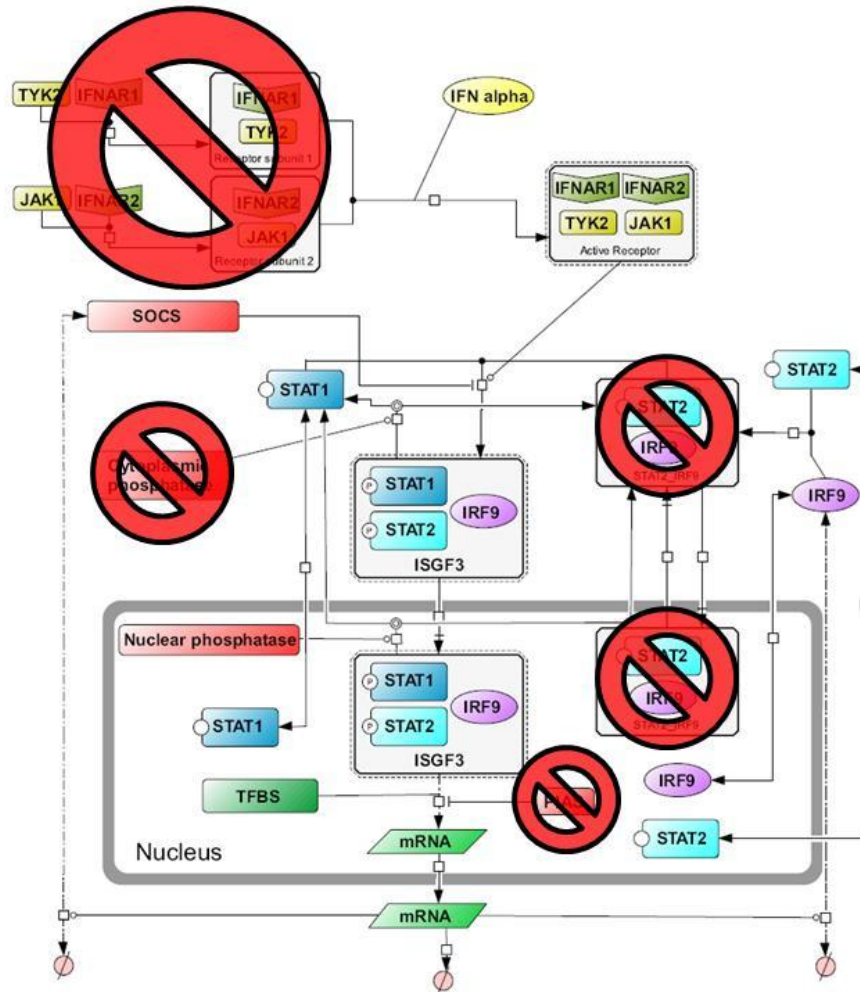


Figure 15 Schematic overview of the reduced IFN- α signalling model. Based on Figure 4. Red signs depict reduced or simplified reactions, namely ligand-receptor binding, feedback by cytoplasmic phosphatases, constitutive binding of STAT2 and IRF9 and feedback by PIAS. For details see Table 6. Lines with empty circles: reaction catalysis; lines with perpendicular bars: reaction inhibition; dotted lines: transcription; TFBS: transcription factor binding site. The scheme was generated using CellDesigner (Kitano et al. 2005).

Results - Model reduction and parameter estimation

Nr.	Reaction	Kinetic rate law
1	IFN_influx -> IFN_free	$k1*s1$
2	IFN_free + Inactive Receptor Complex -> Activated Receptor Complex	$k2*s1*s2$
3	Activated Receptor Complex = Dephosphorylated Receptor Complex	$k3*(s1-(1/k4)*p1)$
4	Activated Receptor Complex + STAT2c -> Receptor_STAT2	$k5*s1*s2$
5	Receptor_STAT2 + STAT1c -> Receptor_STAT2_STAT1	$k6*s1*s2$
6	Activated Receptor Complex -> Inactive Receptor	$k7*s1+k8*s1*modifier(SOCS)$
7	Receptor_STAT2_STAT1 + IRF9c -> ISGF-3c + Activated Receptor Complex	$k9*s1*s2$
8	ISGF-3c -> ISGF-3n	$k10*s1$
9	ISGF-3n + Nuclear phosphatase(NP) = ISGF-3n_NP	$k11*(s1*s2-(1/k12)*p1)$
10	ISGF-3n_NP -> STAT1n + STAT2n + NP + IRF9n	$k13*s1$
11	STAT1n = STAT1c	$k14*(s1-(1/k15)*p1)$
12	STAT2n = STAT2c	$k16*(s1-(1/k17)*p1)$
13	IRF9n = IRF9c	$k18*(s1-(1/k19)*p1)$
14	IRF9n ->	$k20*s1$
15	Open TFBS + ISGF-3n = Occupied TFBS	$k21*(s1*s2-(1/k22)*p1)$
16	NP + Occupied TFBS = Occupied TFBS_NP	$k23*(s1*s2-(1/k24)*p1)$
17	Occupied TFBS_NP -> STAT1n + STAT2n + IRF9n + Open TFBS + NP	$k25*s1$
18	-> mRNAc	$k26*modifier(Occupied\ TFBS)$
19	mRNAc ->	$k27*s1$
20	= IRF9c	$k28+k29*modifier-p1*k20(mRNAc)$
21	-> mRNAc_SOCS	$k30*modifier(Occupied\ TFBS)$
22	mRNAc_SOCS ->	$k31*s1$
23	= SOCS1	$k32*modifier-k33*p1(mRNAc_SOCS)$

Table 6 Overview of kinetic reactions and equations of reduced model. Second column shows reaction formulas. “=” defines reversible reactions, “->” irreversible reactions, respectively. Third column displays according kinetics. Suffixes: c: cytoplasm, n: nucleus. Kinetic rate laws: s: substrate, p: product according to their correspondent reactions.

Results - Model reduction and parameter estimation

Nr.						
1	k1 :	0.997				
2	k2:	0.00504				
3	k3:	0.0241	k4:	43.4		
4	k5:	0.000327				
5	k6:	7.61E-06				
6	k7:	0.00971	k8:	0.118		
7	k9:	0.000153				
8	k10:	0.000938				
9	k11:	0.000224	k12:	100		
10	k13:	1.32E-06				
11	k14:	0.012	k15:	5.11		
12	k16:	0.338	k17:	5.11		
13	k18:	4.07E-05	k19:	3.1		
14	k20:	3.08E-05				
15	k21:	2.51E-06	k22:	0.0105		
16	k23:	0.827	k24:	86.9		
17	k25:	0.108				
18	k26:	1.70E-02				
19	k27:	1.00E-06				
20	k28:	0.001386	k29:	0.00114	k20:	3.08E-05
21	k30:	0.00114				
22	k31:	0.101				
23	k32:	1	k33:	4.98E-05		

Table 7 Overview of kinetic parameters of reduced model. Reactions and kinetic parameters are numbered according to Table 6.

The reduction of the model to 33 parameters only improved the ratio between free parameters and available data points and made it possible to perform a meaningful parameter estimation approach.

Parameter estimations were performed utilizing a custom framework based upon the profile likelihood method (Raue et al. 2009). Using profile likelihood as a tool to perform a parameter estimation analysis combines local fitting algorithms and parameter distortions in a specific workflow. Upon starting a profile likelihood analysis, a single parameter of the input variables is chosen, while all other parameters are fixed at first. The chosen parameter is altered around its initial value within a defined threshold with:

$$parameter = parameter \pm \frac{threshold}{number\ of\ intervals}$$

Once the parameter is set to a different value, it is fixed while all other input variables are used as an input for a local fitting procedure. This step is repeated for each interval within the defined threshold and the resulting scores for each local fit are stored. Visualizing all obtained scores for a single parameter will lead to one of three scenarios (Figure 16):

- a. A straight line depicting no rise in score values (Structurally non-identifiable parameter) (Figure 16B)
- b. A parameter range with a lowest score and a one-sided rise in score values (Practically non-identifiable parameter) (Figure 16D)
- c. A parable, describing a central parameter range with a lowest score and a rise in score values once the parameter value is moved out of this range (Identifiable Parameter) (Figure 16F)

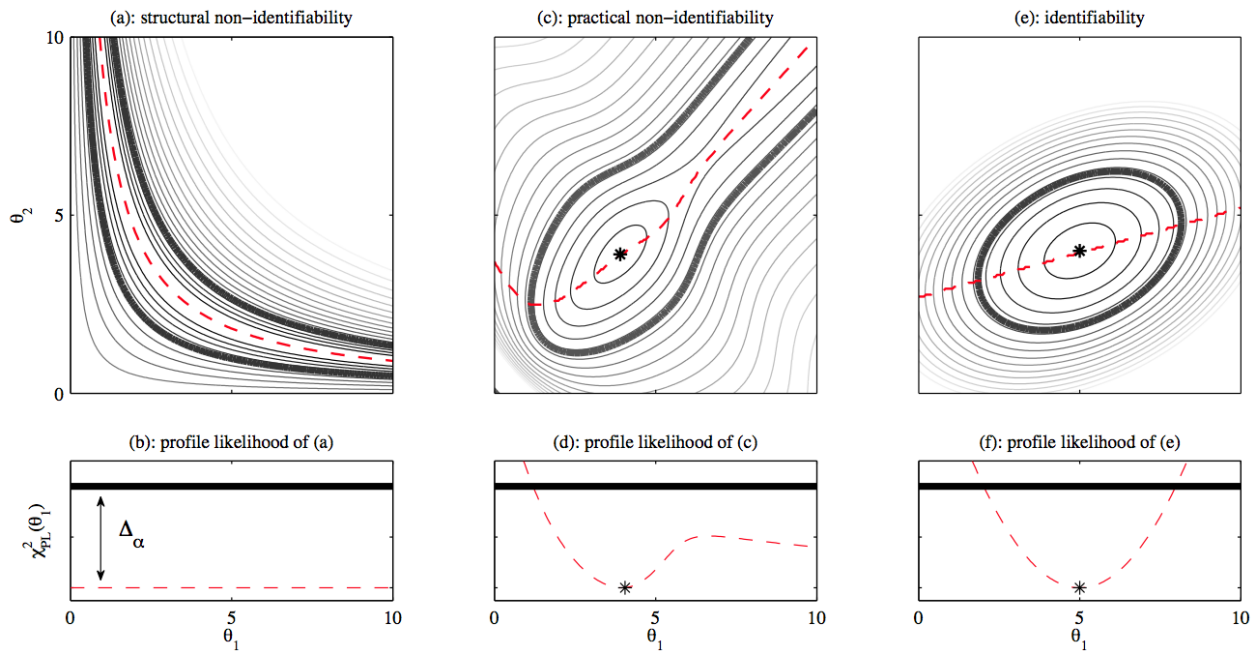


Figure 16 Profile Likelihood Approach. Assessing parameter identifiability of parameter θ_1 from the profile likelihood $\chi^2_{PL}(\theta_1)$ for: **(a)** A structural non-identifiability along the functional relation $h(\theta_1, \theta_2) = \theta_1 * \theta_2 - 10 = 0$ manifesting in a flat profile likelihood in panel **(b)**. **(c)** A practical non-identifiability manifesting in a flattening out of the profile likelihood for $\theta_1 \rightarrow \infty$ in panel **(d)**. A lower confidence bound can be assessed by the point where $\chi^2_{PL}(\theta_1)$ exceeds Δ_α . **(e)** An identifiable parameter θ_1 . The profile likelihood approaches a parabola shape indicating a good approximation by standard intervals in panel **(f)**. **(a,c,e)** Contour lines shaded from black to white correspond to low respectively high values of $\chi^2(\theta)$. Thick contour lines indicate likelihood-based confidence regions and asterisk correspond to the optimal parameters $\hat{\theta}$. Dashed lines indicate the trace of the profile likelihood for θ_1 in terms of parameter values. **(b,c,f)** Dashed lines indicate the profile likelihood χ^2_{PL} of parameter θ_1 . The thick lines display the threshold Δ_α utilized to assess likelihood-based confidence regions for a confidence level α . $\Delta_\alpha = Q(\chi^2_{df}, \alpha)$ is the α -quantile of the χ^2 -distribution with df degrees of freedom. Kindly provided by Andreas Raue (Raue et al. 2011).

Running a global profile likelihood analysis will apply this algorithm to every free parameter in the model. As a result, groups of fitting scores for each parameter are obtained. Then, the lowest score of these values with the according set of fitted parameters can be selected for further optimization approaches until the lowest possible score is reached.

Using this method on the reduced model to estimate the remaining 33 free parameters led to an accurate description of the experimental data by the model (Figure 17). However, afore mentioned results that were obtained during the usage of the profile likelihood algorithm revealed 7 parameters that were characterized as structurally non-identifiable (Figure 18). Structurally non-identifiable parameters are commonly interpreted to indicate the potential for further model reduction approaches. As the expected second reduction of the model was going to be minor and more fragile in comparison to the first approach, a more schematic reduction approach was chosen.

The time-scale-separation task implemented in COPASI is able to identify the speed of each kinetic reaction in the model for different time points and separate the time-scale into fast and slow modes (Surovtsova et al. 2009). Once the time-scale is separated, a participation index for each kinetic reaction is calculated, representing the participation of the respective reaction in each individual mode. If a reaction is identified as fast over a majority of the time-scale of interest, it is likely that this reaction holds no impact on the kinetic behaviour of the model. In that case, a common technique is to lump the according reaction. Lumping refers to bridging the fast kinetic reaction and connecting the adjacent reactions which would make the appointed parameter drop out of the model (Dokoumetzidis et al. 2009). This approach was performed on the reduced model, resulting in a minimal model with 22 free parameters (For a detailed description see [Materials & Methods](#)) (Table 8, Table 9).

Results - Model reduction and parameter estimation

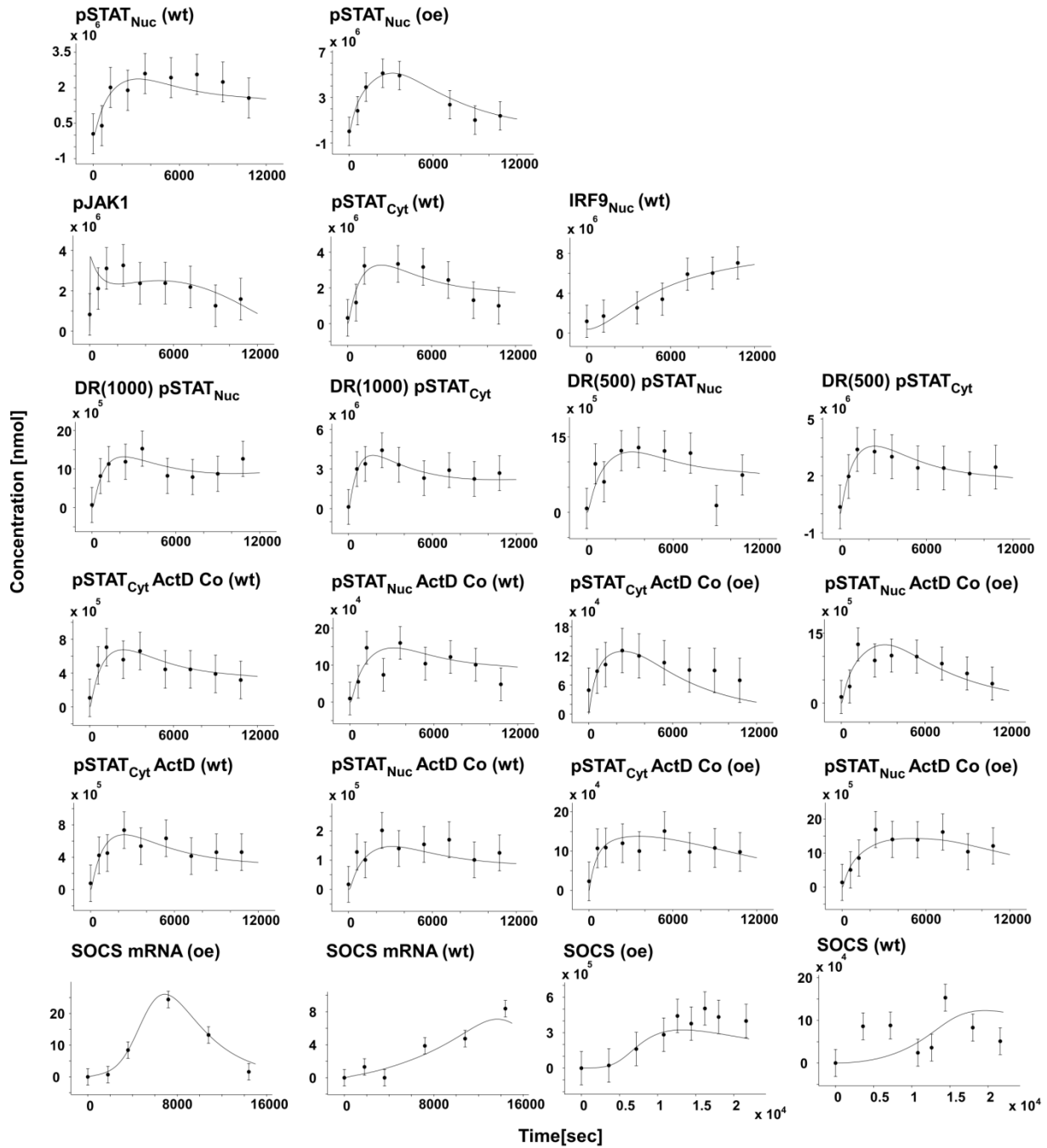


Figure 17 Parameter estimation approach using the reduced model. X-axis describes the time in seconds, y-axis the concentration of the according experimental measurement. Plot titles indicate the performed experiment. Individual data points are shown as dots, error bars depict a standard error. Lines present the kinetic behaviour of the model after the parameter estimation, which is in accordance with experimental data points.

Results - Model reduction and parameter estimation

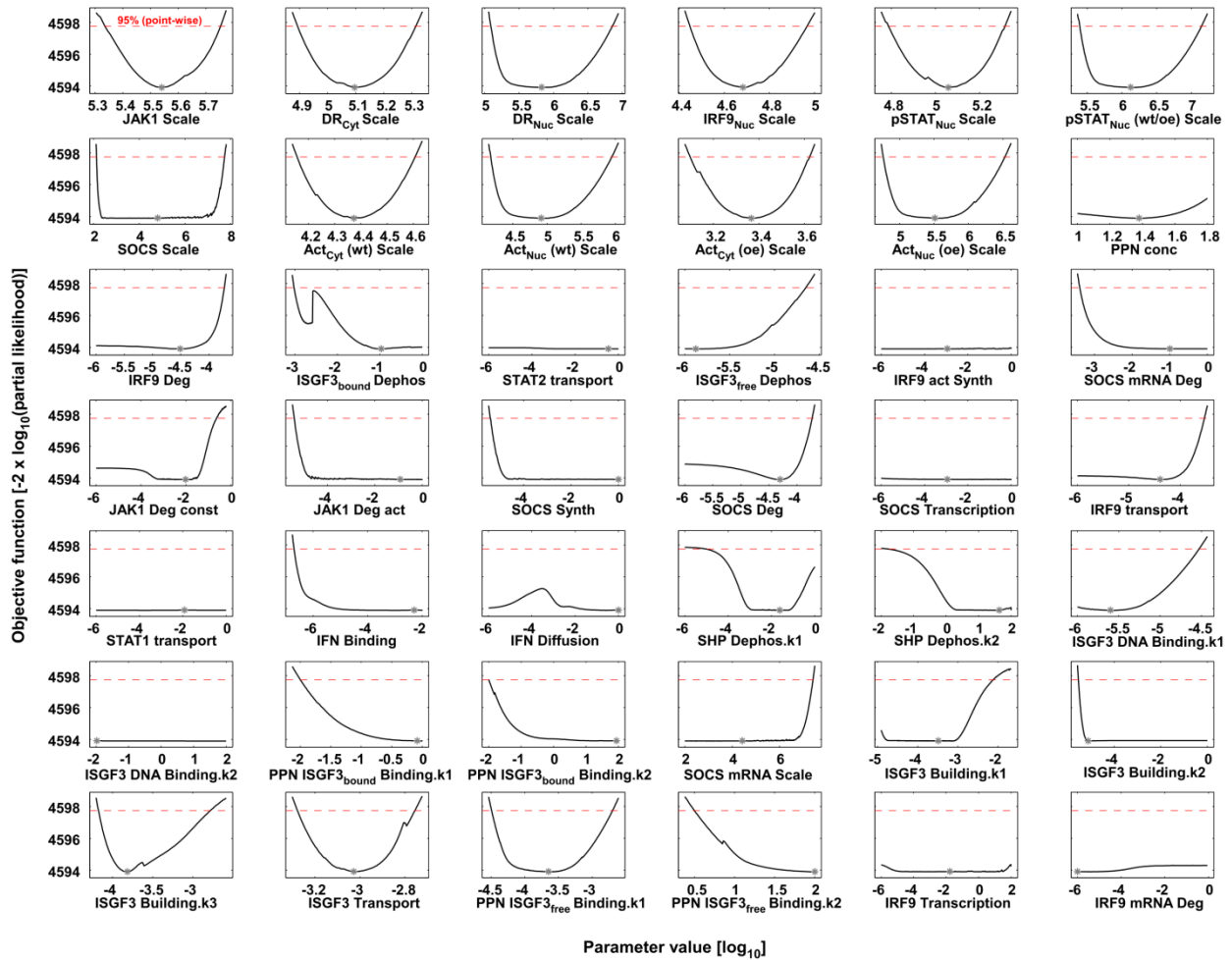


Figure 18 PLE analysis performed on the reduced model. Each plot shows a PLE analysis for one free parameter. X-axis defines the parameter value, y-axis the corresponding objective value. Plot-titles indicate the examined parameter. Plots in the first two rows titled as Scale depict scaling variables for each experiment. 15 parameters are classified as identifiable, 20 parameters are practically non-identifiable and 7 parameters are structurally non-identifiable (Figure 16).

Results - Model reduction and parameter estimation

Nr.	Reaction	Kinetic rate law
1	IFN_influx -> IFN_free	$k_1 \cdot s_1$
2	IFN_free + Inactive Receptor Complex -> Activated Receptor Complex	$k_2 \cdot s_1 \cdot s_2$
3	Activated Receptor Complex + STAT2c -> Receptor_STAT2	$k_3 \cdot s_1 \cdot s_2$
4	Receptor_STAT2 + STAT1c -> Receptor_STAT2_STAT1	$k_4 \cdot s_1 \cdot s_2$
5	Activated Receptor Complex -> Inactive Receptor Receptor_STAT2_STAT1 + IRF9c -> ISGF-3c + Activated Receptor Complex	$k_5 \cdot s_1 + k_5 \cdot k_6 \cdot s_1 \cdot \text{modifier (SOCS)}$
6	ISGF-3c -> ISGF-3n	$k_7 \cdot s_1 \cdot s_2$
7	ISGF-3c -> ISGF-3n	$k_8 \cdot s_1$
8	ISGF-3n + Nuclear phosphatase(NP) = ISGF-3n_NP	$k_9 \cdot (s_1 \cdot s_2 - (1/k_{10}) \cdot p_1)$
9	ISGF-3n_NP -> STAT1n + STAT2n + NP + IRF9n	$k_{11} \cdot s_1$
10	STAT1n = STAT1c	$k_{12} \cdot (s_1 - (1/k_{13}) \cdot p_1)$
11	STAT2n = STAT2c	$k_{14} \cdot (s_1 - (1/k_{15}) \cdot p_1)$
12	IRF9n = IRF9c	$k_{16} \cdot (s_1 - (1/k_{17}) \cdot p_1)$
13	IRF9n ->	$k_{18} \cdot s_1$
14	-> mRNAc	$k_{19} \cdot \text{modifier (ISGF-3n)}$
15	mRNAc ->	$k_{20} \cdot s_1$
16	= IRF9c	$k_{21} + k_{21} \cdot k_{22} \cdot \text{modifier-p}_1 \cdot k_{18}$ (mRNAc)
17	-> mRNAc_SOCS	$k_{23} \cdot \text{modifier (ISGF-3n)}$
18	mRNAc_SOCS ->	$k_{24} \cdot s_1$
19	= SOCS1	$k_{25} \cdot \text{modifier-k}_{26} \cdot p_1$ (mRNAc_SOCS)

Table 8 Overview of kinetic reactions and equations of minimal model. Second column shows reaction formulas. “=” defines reversible reactions, “->” irreversible reactions, respectively. Third column displays according kinetics. Suffixes: c: cytoplasm, n: nucleus. Kinetic rate laws: s: substrate, p: product according to their correspondent reactions.

Nr.					
1	k1 :	6.17E-04			
2	k2:	0.00000129			
3	k3:	2.90E-03			
4	k4:	1			
5	k5:	1.40E-05	k6:	3.57	
6	k7:	8.32E-05			
7	k8:	1.75			
8	k9:	3.63E-05	k10:	3.21E-02	
9	k11:	1			
10	k12:	1.95E-02	k13:	5.11 (fixed)	
11	k14:	1.00E-06	k15:	5.11 (fixed)	
12	k16:	1.18E-04	k17:	3.1 (fixed)	
13	k18:	1.00E-06			
14	k19:	8.61E-05			
15	k20:	1.00E-06			
16	k21:	Calculated from k18	k22:	7.46	k18: 0.000001
17	k23:	3.36E-03			
18	k24:	1.66E-04			
19	k25:	5.05E-06	k26:	9.00E-05	

Table 9 Overview of kinetic parameters of reduced model. Reactions and kinetic parameters are numbered according to Table 8.

The time-scale-separation task has been performed on the reduced model. Results showed that the participation indices of two reactions were classified as fast for 90.9% of the modelled time scale, with only a limited timeframe between 10.000 and 11.000 seconds showing a switch into a dominant participation into slow modes for both reactions (Figure 19). Therefore, constitutive receptor dephosphorylation and binding of ISGF-3 to DNA were selected for further reduction approaches. Following this result, constitutive receptor dephosphorylation was dropped from the model and nuclear accumulation of ISGF-3 and constitutive dephosphorylation by nuclear phosphatases was simplified. Furthermore, for transport reactions of STAT1, STAT2 and IRF9, k_{eq} values were experimentally measured. For this purpose, mentioned molecules were measured in cytoplasm and nucleus without interferon stimulation, and a respective ratio was calculated (Figure 20). Following this result, STAT molecules were assumed to be present at a 23-fold increased concentration in the cytoplasm in comparison to the nucleus, whereas IRF9 molecules are assumed to be present at a 14-fold increased concentration in the cytoplasm in comparison to the nucleus. The obtained minimal model was used again to perform a parameter estimation approach using the aforementioned custom framework by Andreas Raue. Resulting parameter values for the minimal model were able to describe the experimental data with the exception of the measurement of SOCS mRNA in a wildtype environment (Figure 21). For this measurement, the fit does not reach the final data point but starts to drop at the data point at 3 hours. Concluding, the model has been reduced by 33% from 33 free parameters to 22 free parameters. Although the second reduction is not able to describe the data as accurately as the first reduction, a minimalistic model for the IFN- α signalling pathway seems achievable, which is in line with prior results showing that control over the signalling pathway is limited to few decisive molecules.

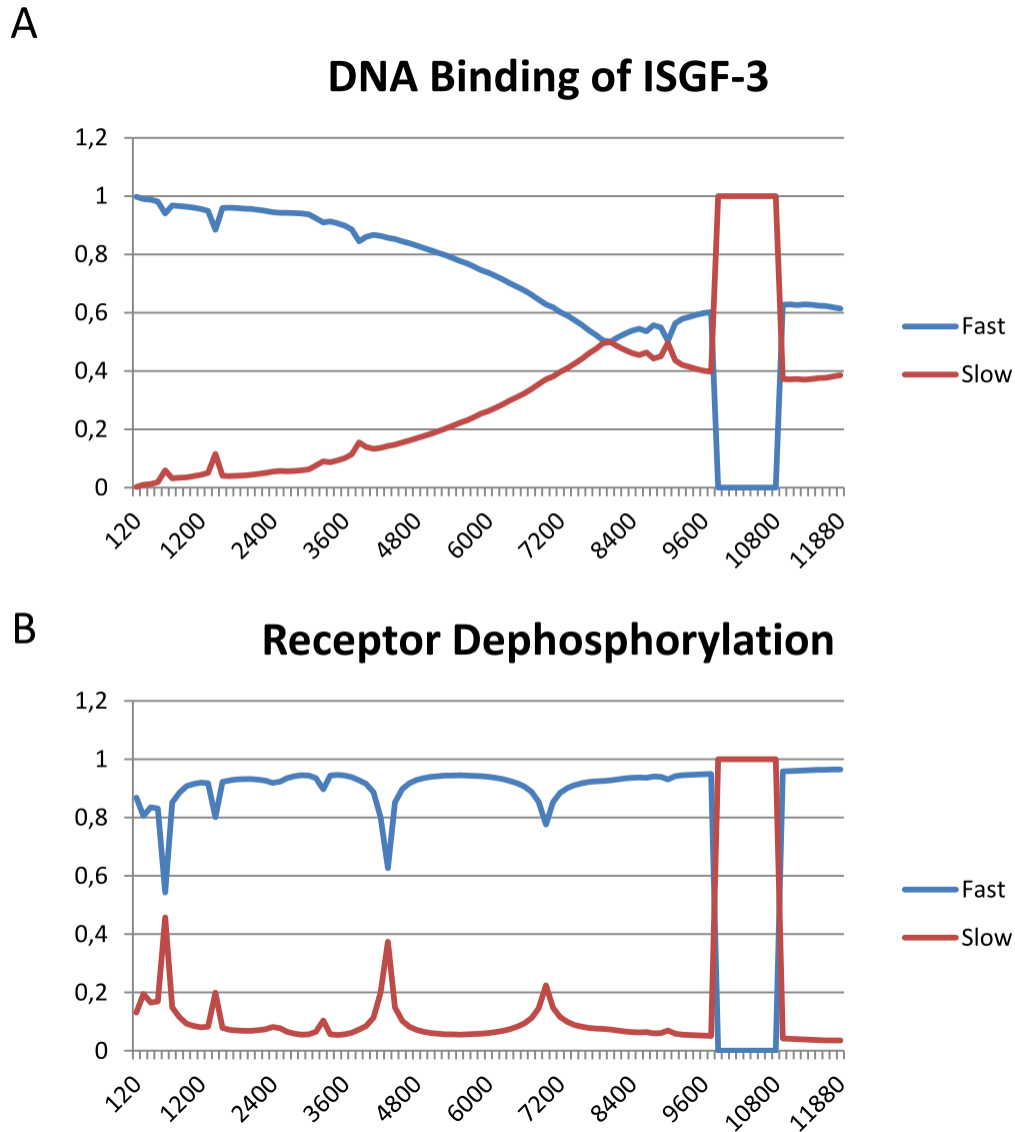


Figure 19 Time Scale Separation analysis of (A) DNA binding of ISGF-3 and (B) Receptor dephosphorylation. X-Axis represents time in seconds, y-axis shows the participation index of the respective reaction for fast modes (blue line) and slow modes (red line). In detail, the normalized sums of all participation indices for fast modes and for slow modes have been calculated for each time point. For both reactions 90.9% of the time points show a dominant participation of the reaction into the fast modes.

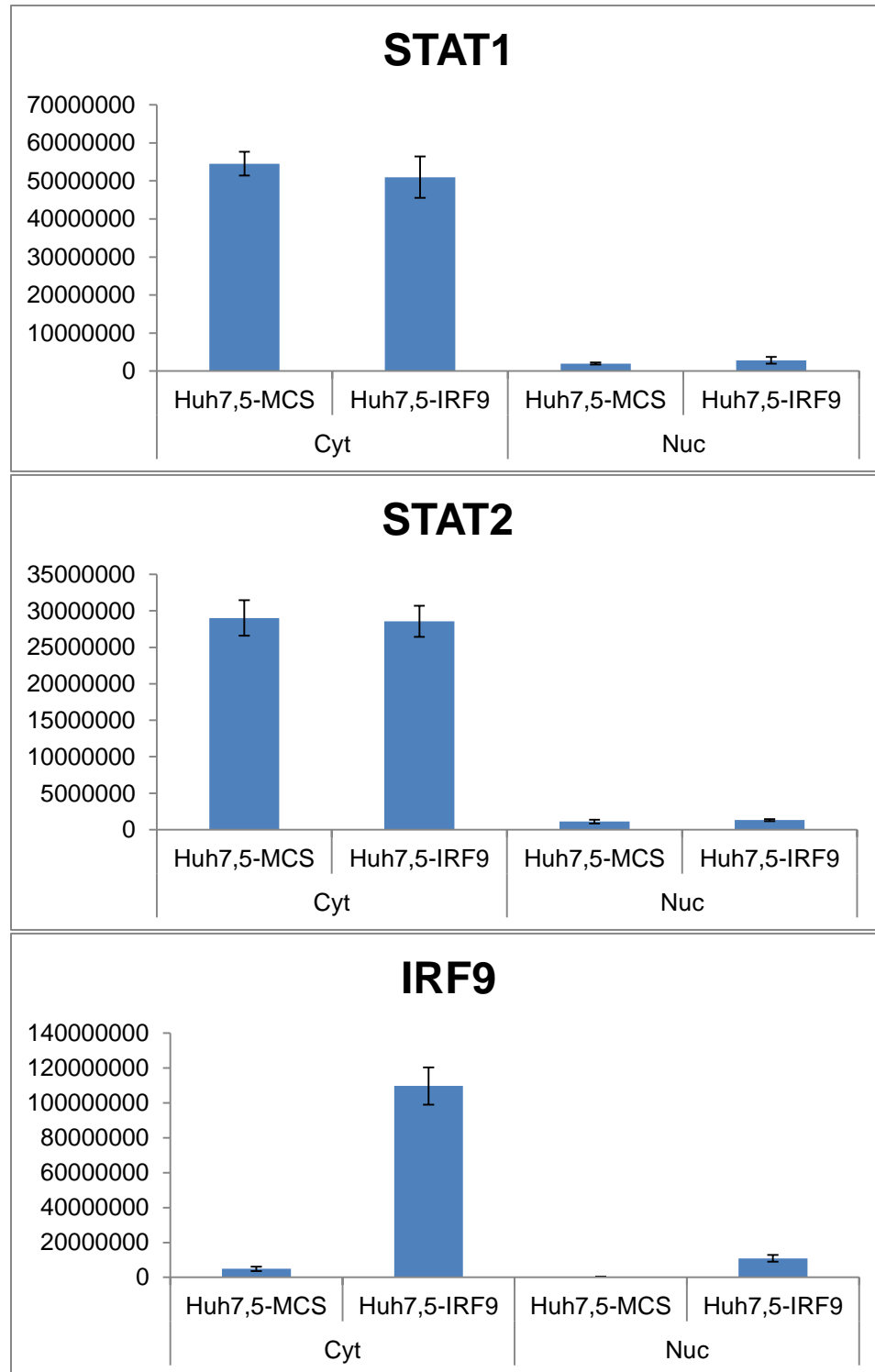


Figure 20 Calculation of the ratio of STAT1, STAT2 and IRF9 molecules between cytoplasm and nucleus. X-Axis describes the respective measurement for wildtype cells (MCS) or IRF9 overexpression cells (IRF9) in cytoplasm (cyt) or nucleus (nuc). Y-axis shows the measured concentration. Four measurements were obtained and the average is depicted by the blue bars. Error bars represent the standard deviation between those experiments. Ratios calculated from the measurements are: STAT1 and STAT2: 23-fold increased concentration in cytoplasm compared to nucleus. IRF9: 14-fold increased concentration in cytoplasm compared to nucleus.

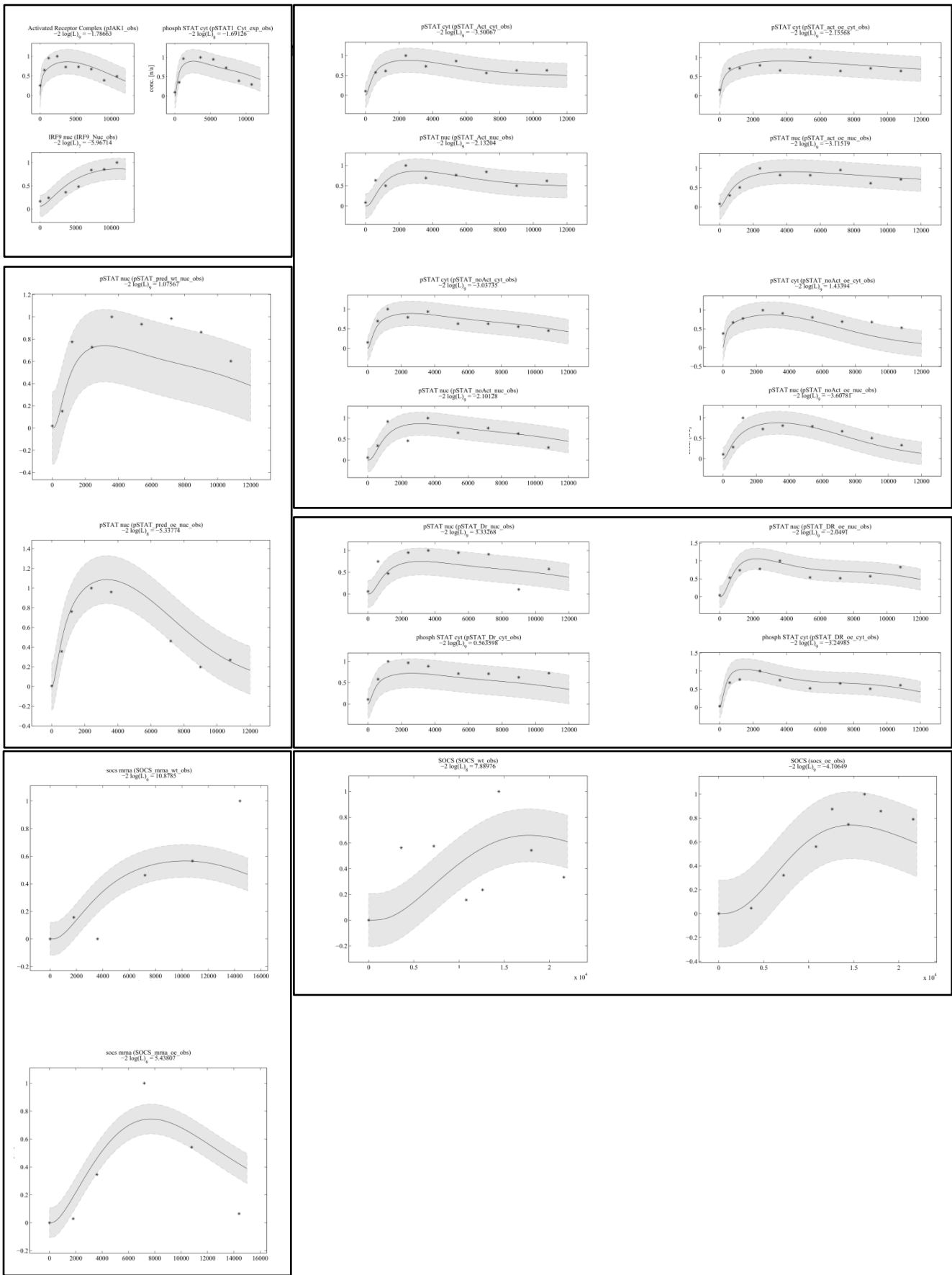


Figure 21 Parameter estimation approach using the minimal model. X-axis describes the time in seconds, y-axis the concentration of the according experimental measurement. Plot titles indicate the performed experiment and the calculated fitting score for the respective measurement. Individual data points are shown as dots, grey areas depict a standard error. Lines present the kinetic behaviour of the model after the parameter estimation. Black frames indicate experimental measurements that belong together.

DISCUSSION

IDENTIFICATION OF KEY MOLECULES AND REACTIONS OF THE IFN ALPHA PATHWAY

In this thesis, a mathematical model for the IFN- α signalling pathway has been developed. The focus of the modelling process was to find every known interaction of the JAK/STAT signalling pathway from literature and combine this knowledge into a comprehensive model. The rate law interpretation of the model is assumed to be deterministic. Arguably, a stochastic approach would have been appropriate for modelling a signal transduction network, as concentrations of involved molecules are low. Therefore, a stochastic interpretation of the used rate laws is more likely to describe real life behaviour of single cell signalling dynamics. However, as all experimental measurements were retrieved from cell populations, it is reasonable to simplify the model behaviour towards a deterministic view. Using this model, key molecules and reactions should be identified and proposed for further experimental measurements. Specifically, perturbing the signalling pathway to change the kinetic behaviour of the system and possibly enhance the anti-viral functionality was aimed for. Obviously, a mathematical model including all known negative and positive feedbacks represents an underdetermined system as it contains too many parameters to be reliably estimated from the experimental data. To verify the predictive power of the model, a sensitivity analysis of 1000 parameter sets describing the experimental data was performed and results were compared to the original parameter set (Figure 7). The major observations were comparable, indicating that they are intrinsic properties of the model structure. Robustness of sensitivity against single parameter changes has been described by Gutenkunst et al. (Gutenkunst et al. 2007), suggesting that model predictions are reasonable when they are derived from collective fits and can only be improved by precise and complete measurements of all kinetic parameters. Analysis of the sensitivity calculation led to the understanding that few reactions and protein concentrations were decisive for the kinetic behaviour of the signalling pathway. These

mechanisms included constitutive negative feedback by nuclear phosphatases, induced negative feedback by SOCS proteins and concentration of IRF9. Especially raising the level of IRF9 showed a positive influence on the amount of signalling as well as the response time (Figure 9A), which is proposed to be crucial for the outcome of an anti-viral reaction. This effect was experimentally validated, proving concentration, synthesis and degradation of IRF9 to be critical for signalling properties like the area under curve or the time of the peak (Figure 9B). Increasing the initial IRF9 concentration by overexpression resulted in higher levels of phosphorylated STAT proteins in the nucleus and consequently in augmented expression of IFN alpha target genes. This is consistent with previous reports describing the impact of IRF9 on the amount of active ISGF3 (Bandyopadhyay et al. 1990; Levy et al. 1990; Weihua et al. 2000; Tamada et al. 2002). However, distinct from previous studies, analysis of the IFN response was performed in a time resolved manner. Analysis showed that enhanced IFN induced gene expression not only applies for isolated time points but rather for the overall integrated response. In addition, it was demonstrated that IRF9 is also crucial for the speed of IFN response, with higher IRF9 levels accelerating signal transduction and gene expression. Theoretically, these effects of IRF9 could be achieved by two mechanisms: by increased nuclear import of the signal transducers or by IRF9-mediated protection from nuclear phosphatases. Model analysis excluded accelerated nuclear import and indicated protection from nuclear phosphatases as the underlying mechanism. In detail, model simulations were in accordance with literature over the importance of generous nuclear phosphatases (Smieja et al. 2008) and specifically requiring the effect of nuclear phosphatase protection through DNA-binding to accurately predict the kinetic of an IRF9 overexpression (Figure 9C) (Meyer et al. 2003).

In summary, inhibition of nuclear phosphatases, inhibition of induced negative feedbacks and overexpression of IRF9 were classified as valuable targets to strengthen the effectiveness of IFN- α signalling. However, nuclear phosphatases are known to be redundant and even a knock-out of the most prominent molecule TC45 does not lead towards a significantly lower nuclear phosphatase activity (ten Hoeve et al. 2002). Taking this into account, the focus shifts upon the

induced feedback mechanisms. Concluding, an alteration of those induced feedback mechanisms provides the opportunity to influence the outcome of the IFN- α signalling pathway.

ANALYSIS OF GENETIC RESPONSE PATTERN

Overexpression of IRF9 has been shown to have a major impact on the kinetic response of the JAK/STAT signalling pathway. To learn about following effects of this alteration, the genetic response for wild type cells and IRF9 overexpression cells has been analysed. Therefore, an array experiment was performed in collaboration with Annette Schneider and Norbert Gretz. Analysis of the results was performed by Hauke Busch (Figure 11). It showed that wildtype and IRF9 overexpressing cells displayed different expression kinetics of the analysed genes. For instance, SOCS1 expression was rapidly activated and repressed, whereas the activation of USP18 was sustained. These observations are concordant with a recent report stating that SOCS1 is responsible for early inhibition of IFN alpha signalling, whereas USP18 mediates late inhibition (Sarasin-Filipowicz et al. 2009). Currently, possible explanations for this diverse genetic response are under investigation. Explanations which have been mentioned earlier include a transcription factor network, where specific transcription factors could selectively upregulate certain genes over a prolonged timeframe. A bioinformatical analysis using STRING database supports this theory, as results predict IRF1 as the central node in a potential regulatory network (Figure 12). IRF1 is a well-studied hub-gene, known to regulate a variety of different biological processes. Among others, supporting the cellular anti-viral response is the most prominent function of IRF1. Furthermore, IRF1 binds to a consensus sequence that is highly similar to the ISRE. Therefore, several indications point towards an involvement of IRF1 as a regulatory factor of the interferon alpha induced gene response.

Another theory is based on auto stimulation of cells by releasing a potent ligand upon IFN- α stimulation. For example, small doses of IFN- α could be secreted from the cell and restimulate the system. In that case, selective expression of IFN- α induced genes would be explained by specificity of transcription factor binding sites, i.e. sustained genes would show a high specificity towards ISGF-3, whereas bursting genes present a low specificity, respectively. The third theory involves miRNA based regulation mechanisms, e.g. induced miRNAs could interfere with the transcription of specific mRNAs which would lead to a selective response at later time points after the stimulation. The last explanation takes into account the different stability rates of mRNA. After a single stimulus, certain mRNA could start a short time response before they get actively degraded, whereas more stable mRNA could be used for translation over a prolonged period. As mentioned before, these theories could work together in synergy, making it a difficult task to distinguish single effects. Therefore, further analysis combining model simulations and experimental measurements is required to improve our understanding of genetic regulatory effects of IFN- α signalling.

MEDICAL IMPACT

As mentioned before, IFN- α is used as a treatment of hepatitis C and B virus infection and leads to an uncertain outcome as the effectiveness of the treatment is highly patient dependent (Manns et al. 2001). Differences that might be responsible for the diverse outcome of the treatment have not been identified, but are under investigation (Chen et al. 2005; Sarasin-Filipowicz et al. 2008). However, it is tempting to speculate that a highly sensitive part of the signalling cascade will likely have an impact on the decision process whether to respond or not. In that case, previous results could be used to support IFN- α treatment. For instance, measuring the concentration of IRF9 protein from a tissue sample and comparing responder and non-responder patients might be able to provide further insights into the medical use of IFN- α treatment. A difference in IRF9

concentration could be used as a screening method to identify responders prior to the actual IFN- α treatment. Following this idea, given the opportunity to artificially raise the IRF9 levels of a patient before IFN- α treatment could lead to a transition of non-responders into responders. To sum up, previous results identifying decisive reactions and protein concentrations for the IFN- α signalling cascade should be validated *in vivo* and might therefore lead to an improvement of the medical use of IFN- α .

SENSITIVITY-BASED MODEL REDUCTION AND PARAMETER ESTIMATION

Focusing on the theory that few decisive molecules are responsible for the kinetic outcome of the IFN- α signalling pathway, a two-step model reduction and parameter estimation approaches have been performed. First, several local fits using the full model were obtained. Parameter values of the resulting fits were compared and their respective coefficients of variation were calculated. A high variation of a free parameter is interpreted as not having a major impact on the kinetic behaviour of the signalling dynamics, whereas a low variation indicates that the individual parameter has to be conserved within a certain range to ensure a good fit of the data-points. Parameters were sorted by their according coefficient of variation and parameters with high variations were fixed. This analysis showed that reducing the number of free parameters to 33 only was still able to fit the experimental data accordingly. Therefore, the first reduced model was built by keeping the parameters with a low coefficient of variation while dropping or simplifying the parameters with a high coefficient of variation.

This sensitivity-based method for model reduction was chosen as the original model was meant to be comprehensive and a major decrease of free kinetic parameters was aimed for. Obtaining a list of parameters which have been sorted according to their probability to influence the pathway offered the possibility to test several reduced model structures by adjusting the threshold of imported parameters of the original model. Following the selection of the most influential

parameters and setting up the reduced model, parameter estimations were performed using a custom Matlab based framework by Andreas Raue. As described earlier, the approach is based upon several local fitting calculations with randomly disturbed starting parameters. Furthermore, the analysis can be supported by a profile likelihood analysis, suggesting single parameter values that could lead towards improved fitting scores. Another approach was using the parameter estimation task implemented in Copasi, where different local and global fitting algorithms can be selected to find the most optimal algorithm for the given problem. However, global fitting algorithms in Copasi were not able to find minima in the same order of magnitude score-wise as the multi-start local fitting approach. Local fitting algorithms implemented in Copasi were outperformed by the Matlab-based framework, as a single local fit was less time demanding, reasoning the choice of the computational tool.

The resulting reduced model was able to accurately fit the experimental data. As another result of the reduction, reactions that can be simplified or dropped without losing the potential to fit the experimental data accurately are likely to have a similar low impact during the biological signal transduction for the respective environment in which experimental measurements have taken place. For instance, pre-association of STAT2 and IRF9 before interferon stimulation was dropped in the reduced model, pointing towards the idea that this effect does not play a major role in IFN- α signalling for the observed timeframe. Another example is the reduction of cytoplasmic phosphatases: As ISGF-3 accumulation in the nucleus is assumed to be a fast process, the role of a constitutive negative feedback is assumed by nuclear phosphatases. Looking at the biological impact of this result, an inhibition of cytoplasmic phosphatases is likely to have a minor effect on the observed signalling cascade. Finally, the exclusion of phosphorylated STAT dimers was performed, as it is assumed in the model that these complexes have no influence on the transcriptional activity if they are not bound to IRF9. Under this circumstance, activated STAT dimers do not have an impact on the induced feedback response of the system and therefore comprehend no major control over the global system kinetics.

TIME SCALE SEPARATION BASED MODEL REDUCTION AND PARAMETER ESTIMATION

As a further approach to decrease the number of free parameters in the model, a second model reduction has been performed. For the reduction to a minimal model, a more precise identification of reducible reactions was aimed for. Instead of using the sensitivity-based identification of non-conserved kinetic parameters, the time-scale separation task implemented in Copasi has been utilized. The analysis identified two reactions that were fast over 90.9% of the modelled time scale, namely constitutive receptor dephosphorylation and ISGF-3 binding to DNA. Therefore, receptor dephosphorylation has been dropped from the model and the reactions involving ISGF-3 in the nucleus have been simplified, resulting in a 33% decrease of free parameters between the first reduced model and the minimal model. The simplification of nuclear ISGF-3 concentration, which is transcriptionally active without binding of DNA in the minimal model, involved the reduction of constitutive negative feedback by nuclear phosphatases to a single reaction.

However, the minimal model has not been able to describe the experimental data as accurately as the first reduced model. Looking at the measurement of SOCS mRNA in the wildtype environment (Figure 21), the model predicts a decrease of the mRNA concentration before the final data point. Taking into account that all remaining data points (approximately 180), with the exception of aforementioned data point, were fitted accurately, it seems likely that a minimal model describing all experimental measurements is achievable. Interestingly, looking at the predictions obtained by the full model, phosphatase protection by ISGF-3 binding to DNA was required to accurately describe the kinetic behaviour of signalling responses in wildtype cells and IRF-9 overexpression cells. Although the model has been drastically reduced, the mechanism of phosphatase protection could still be decisive to fit the experimental data, despite being identified as dominant fast reactions. Another reason for the suboptimal parameter fitting approach could be presented in Figure 19: 90.9% of the calculated time points were classified as dominant in the fast modes, but both reactions show an area between 10.000 and

11.000 seconds where the dominant participation changes and both reactions are classified as majorly contributing to the slow modes. Although this behaviour affects only a limited time-frame, a reduction of those reactions might not be compensatable for the remaining reactions in the minimal model.

To obtain a minimal model that is able to fit all experimental data and therefore identify the core reactions and molecules influencing the IFN- α signalling pathway, further computational analysis is required. The structure of the minimal model has to be enhanced and other tools for identification of reducible parameters should be utilized.

Concluding, the two-phase reduction approach confirmed earlier results, as constitutive negative feedback by nuclear phosphatases and induced feedback mechanisms by IRF9 and SOCS remained decisive controllers of the system throughout both reductions. Alteration of these three mechanisms is proposed to induce strong responses by the biological signalling cascade, turning them into the most valuable targets for further studies to exert control over the IFN- α signalling pathway.

MATERIALS & METHODS

MODELLING

The IFN alpha model was created and graphical outputs of kinetic behaviours of the model were produced using Copasi (Hoops et al. 2006). All reactions are defined as ordinary differential equations. Time course data was computed using the deterministic LSDOA algorithm (Petzold 1983) provided by Copasi. Copasi has been chosen as a modelling environment, as model creation and alteration is implemented in a user-friendly way by a graphical user interface. Furthermore, SBML support should allow file compatibility between other modelling environments (Hucka et al. 2003). Copasi offers a variety of different tasks to work with the model and analyse its kinetic behaviour. For this project, modelling tasks that have been used include time course calculation, sensitivity analysis, parameter estimation, parameter scanning and time scale separation, all of which usually require individual tools to be used. Concluding, Copasi offers an ideal base to start and work with a new modelling project.

A detailed overview of the specific reactions defined in the full model is provided in Table 1 and kinetic parameters are depicted in Table 2. The reduced model is presented in Table 6 and Table 7, respectively. The minimal model is shown in Table 8 and Table 9.

Sensitivity analyses of the model were performed via numerical differentiation of simulation results by finite differences (Sahle et al. 2008). The calculation is defined as:

$$c_x^y = \left(\frac{\Delta y}{\Delta x} * \frac{x}{y} \right)_{\Delta x \rightarrow 0}$$

For the approach presented in this thesis, Δx describes the change of initial concentrations of model species, whereas Δy stands for the resulting change of the specified kinetic behaviours that were selected as an output function, namely

the time of the signalling peak and the area under the curve of the ISGF-3 concentration in the nucleus.

Obtaining several valid parameter sets was achieved by using the random search algorithm implemented in Copasis optimization task. In detail, all model parameters were varied randomly between +/- 50% of their original value. For selection, the resulting kinetic behaviours had to match the experimental data. Matching was determined by several criteria: (i) The amount of maxima in the kinetic behaviour had to be identical. (ii) The initial and final concentration, as well as the time and height of peak of each simulated species had to fit into a +/- 20% threshold of the measured data. In general, out of 10000 evaluated parameter sets approximately 1000 valid sets could be retrieved.

Further analysis of the full model was performed using Potterswheel (Maiwald et al. 2008). Potterswheel was developed with the purpose to estimate kinetic parameter values from experimental data. Therefore, Potterswheel is a modelling environment specialised on one individual task. This definition distinguishes Potterswheel from other modelling tools, i.e. Copasi, which tries to offer a wide variety of tasks. However, focussing on one task, Potterswheel offers comfortable tools and presentations for local fit sequence performance and analysis. For this thesis, standard outputs of Potterswheel have been used for local fit sequence analysis depicted in Figure 14 and Table 5. Especially for analysis of individual score-wise parameter differentiation between similar parameter sets as shown in Table 5, Potterswheel offers an ideal set of computational tools. SBML conversion of the model into Matlab format was performed using SBML online conversion provided on the Potterswheel website (<http://www.potterswheel.de>). Additional modifications of the conversion were required and performed manually. 183 local parameter fits were obtained by using the F2 function implemented in Potterswheel. A single fit in Potterswheel stands for single execution of a local Levenberg-Marquardt fitting algorithm (Marquardt 1963). Levenberg-Marquardt is a gradient descent method. It is a hybrid between the steepest descent and the Newton method (Battiti 1992). While the Newton method converges quadratically towards a minimum in its vicinity using the gradients calculated from the functions first and second derivatives, it may not converge if the minimum is far away of the

initial parameter values. In that case, the Levenberg-Marquardt algorithm changes into a steepest descent algorithm, converging only linearly towards a minimum by calculating only the first derivatives of the function, but the algorithm is guaranteed to converge. By definition, the Levenberg-Marquardt algorithm is only capable of finding the closest minimum surrounding the starting point in parameter space. To overcome this limitation, the F2 function in Potterswheel uses multiple procedures of this local fitting algorithm while disturbing the initial starting parameters with a defined strength. Therefore, given that enough fitting procedures were calculated to cover the parameter space of interest, it is likely that a group of single fitting procedures will converge into the global minimum.

Data and plots of the fit group analysis were retrieved with the linear fit sequence analysis function implemented in Potterswheel.

Parameter estimation of the reduced model was performed using a custom, Matlab-based framework by Andreas Raue. Utilizing the profile likelihood method (Raue et al. 2009), the framework was used to perform an identifiability analysis on the reduced model (Figure 18). Results of this analysis are used as starting points for a modified parameters estimation function implemented in the framework. Similar to Potterswheel, the framework implemented by Andreas Raue is focused on a single task, namely estimation of model parameters to describe experimental data. While sharing the same tools for local fitting procedures with Potterswheel, namely the multi-start local Levenberg-Marquardt fitting algorithm with randomly disturbed initial parameters, the custom Framework involves identifiability analysis of the kinetic parameters of the model to support the local fitting algorithm. This combination of both methods increases the possibility of the parameter fitting approach to find the global minimum of the parameter landscape.

Model reduction was supported by the time scale separation task implemented in Copasi. Time Scale Separation was performed using the CSP method (Surovtsova et al. 2011, submitted). As a setup, ratio of modes separation was set to 0.9, maximum relative error to 0.01 and maximum absolute error to 0.001. The analysed timeframe was defined as 12000 seconds with 100 intervals at an interval size of 120.

SENSITIVITY BASED MODEL REDUCTION

For the first reduction of the model, parameters that were fixed during the parameter estimation approach explained earlier were eliminated or simplified. Furthermore, it was aimed to reduce the model to 33 parameters, while preserving the main features of the model. The receptor-based subgroup of reactions was simplified by eliminating the species of kinases JAK and TYK and their according receptor subunits, respectively. Consequently, the receptor is assumed to be inactive but in a dimeric, kinase-associated form and that receptor activation is directly induced by free interferon (Table 6, reaction 2). Binding of STAT molecules to the receptor has been transformed into irreversible reactions (Table 6, reaction 4 / 5). Phosphorylated STAT molecules are assumed to be in complex with IRF9 all the time, which eliminates the cytoplasmic and nuclear species of phosphorylated STAT1/STAT2 heterodimers. This change required a small modification to the process of ISGF3 complex building, now being summarised in a single reaction (Table 6, reaction 7). mRNA of IRF9 and SOCS is now produced directly into the cytoplasm (Table 6, reaction 18 / 21). Species representing cytoplasmic phosphatases (CP) and PIAS as well as all reactions involving these species were deleted. As a general concept, all reversible reactions that were described by mass action kinetics in the full model were modified to

$$k_1 * \left(substrate - \frac{1}{k_2} * product \right)$$

Using these modified mass action kinetics, the reaction is no longer defined by two independent variables k_1 and k_2 , but rather by one independent variable k_1 and one dependent variable k_2 . Consequently, this technical modification leads to an improved performance of parameter estimation algorithms.

TIME SCALE SEPARATION BASED MODEL REDUCTION

For the second model reduction, reducible reaction parameters were identified using the time scale separation task implemented in Copasi (for details on the method and setup, see [Modelling](#)). For this purpose, participation indices for each reaction were calculated over a time scale of 12.000 seconds and for each interval, a dynamic amount of fast modes was separated from the complete time scale. Following, the sums of all fast and slow modes for each interval step were calculated and normalized with:

$$\begin{aligned}\sum fast\ modes + \sum slow\ modes &= \sum all\ modes \\ \frac{\sum fast\ modes}{\sum all\ modes} &= \sum fast\ (normalized) \\ \frac{\sum slow\ modes}{\sum all\ modes} &= \sum slow\ (normalized)\end{aligned}$$

After normalization, sums of fast and slow modes were compared for each time point. If the sum of fast modes increases the sum of slow modes, the individual time step is marked with a “1”, otherwise the time step is marked with a “0”. The average of these marks is calculated and used as a ratio of participation in fast modes against participation in slow modes for each reaction.

Receptor dephosphorylation and binding of ISGF-3 to DNA were calculated to be fast over 90.9% of the time scale of the model simulation. Therefore, receptor dephosphorylation was dropped from the reduced model (Table 6, reaction 3). Furthermore, ISGF-3 is assumed to induce transcriptional activity directly, replacing the species “Occupied DNA binding sites” in both transcriptional reactions (Table 8, reaction 14 and reaction 17). Consequently, ISGF-3 binding to DNA was dropped from the model (Table 6, reaction 15), including the species “Open DNA binding sites” and the following negative feedback by nuclear phosphatases (Table 6, reaction 16 and reaction 17). Two reactions were modified: Receptor degradation (Table 8, reaction 5) and IRF9 synthesis (Table 8, reaction 16) both include a constant parameter as well as an additive term dependent on a modifier:

$$k_{constant} + k_{activated} * modifier$$

To decrease the orders of magnitude of $k_{activated}$ during the fitting process, both reactions have been modified to:

$$k_{constant} + k_{constant} * k_{activated} * modifier$$

Using these modified rate laws, fitting borders for $k_{activated}$ have been limited to:

$$0 < k_{activated} < 10$$

Furthermore, certain parameters have been fixed to specific values. First, constant synthesis of IRF9 has been fixed to represent a 45-fold increase of constant IRF9 degradation for the wildtype environment or a 900-fold increase for the IRF9 overexpression environment (Table 9, reaction 16, k18 for degradation and k21 for fixed constant influx). This modification leads to a constant base level of IRF9 which is expected to be found in the cell before IFN stimulation. This base level can be altered by increased modifier concentrations, i.e. by activated transcriptional activity. For transport reactions of STAT1, STAT2 and IRF9, k_{eq} values were experimentally measured (Figure 20). STAT molecules were assumed to be present at a 23-fold increased concentration in the cytoplasm in comparison to the nucleus, whereas IRF9 molecules are assumed to be present at a 14-fold increased concentration in the cytoplasm in comparison to the nucleus. Therefore, k_{eq} parameters were set accordingly to represent the measured ratios under a non-stimulated environment (Table 9, reaction 10, k13, reaction 11, k15 and reaction 12, k17).

STRING DATABASE

As a bioinformatical approach to analyse the gene-specific response pattern following interferon alpha stimulation, the STRING database was used for predictions of protein-protein interactions. The STRING database uses the combination of several sources, i.e. experimental data and text-mining algorithms, to predict a probability for a specific protein-protein interaction and score this interaction accordingly. For the analysis the highest possible threshold was used (0.9). As an input, all induced genes of the array experiment that showed a bursting or a sustained kinetic behaviour were selected (Table 10). After a first analysis using the STRING database, genes that showed no interaction were dropped from the input and the analysis was repeated.

apol2	EIF2AK2	lamp3	samhd1
apol6	erap2	lba1	sdpr
apol6	gbp1	lgals3bp	sos1
bst2	gbp1	mab21l2	sp100
btn3a1	gnb4	mlkl	sp110
btn3a2	herc5	mx1	stat1
c19orf66	herc6	myd88	stat2
c5orf39	herc6	nmi	tap1
casp7	hla-e	oas1	tap1
cd274	ifi44	oas2	tap2
cd274	ifi44l	oas3	tdrd7
cd38	ifi6	oasl	tlr3
ceacam1	ifih1	parp14	tmem62
cmpk2	ifit1	parp14	tnfsf10
cxcl10	ifit2	parp9	tnfsf10
cxcl11	ifit3	plscr1	trim21
cyp1a1	ifit5	pml	trim22
cyp1b1	ifitm1	pric285	trim25
ddx58	ifitm2	prkd2	txnip
ddx58	ifitm3	psmb8	ube2l6
ddx60	ifitm3	psmb9	usp18
ddx60l	irf1	rbm43	xaf1
dtx3l	irf9	rsad2	zc3hav1
egr1	isg15	samd9	znfx1

Table 10 Genes used as an input for the STRING Database. Bold names have been selected for the second analysis as they were predicted with at least one interaction.

ESTIMATION OF GENE INDUCTION TIMES

Estimations of gene induction times were obtained by Hauke Busch by fitting the mRNA fold expression $g(t)$ to a logistic function:

$$g(t) = \alpha \frac{1}{1 + \exp(\beta - \gamma t)}$$

Parameters α , β and γ were estimated by using a Levenberg-Marquardt nonlinear least-squares algorithm. The start of gene regulation was defined as the time of maximal change in the acceleration of the fitted function; i.e. upregulation time for each gene was defined as the time of maximal acceleration of the logistic function $g(t)$, which is calculated from the first maximum of the third derivative of $g(t)$ (Zaslavsky et al. 2010). The mean difference of gene expression time series was calculated from the mean of the fold expression differences at the respective experiment time points.

ABBREVIATIONS

CP: Generic Cytoplasmic Phosphatases

DNA: Deoxyribonucleic acid

EGF: Epidermal growth factor

Epo: Erythropoietin

Full Model: Comprehensive Model, incorporating of all known feedback mechanisms, 61 free parameters

GAS: Interferon-gamma activated sequence

IFN: Interferon

IFNAR: Interferon- α/β receptor

IL-6: Interleukin 6

IRF9: Interferon regulatory factor 9

ISG56: Interferon stimulated gene 56

ISGF3: Interferon stimulated gene factor 3

ISRE: Interferon stimulated response element

JAK: Janus Kinase

KIR: Kinase inhibitory region

Minimal Model: Derived from Reduced Model using time-scale separation, 22 free parameters

Mx1: Myxovirus resistance 1

NP: Generic Nuclear Phosphatases

PIAS: Protein inhibitor of activated STAT

Abbreviations

PKR: Protein kinase RNA-activated

Reduced Model: Derived from Full Model using an sensitivity-based approach, 33 free parameters

SHP: Src homology region 2 domain-containing phosphatase

SOCS: Suppressor of cytokine signalling proteins

STAT: Signal Transducer and Activator of Transcription

TFBS: Transcription Factor binding sites

TSS: Time Scale Separation

TYK2: Tyrosine Kinase 2

USP18: Ubiquitin specific peptidase 18

CITATIONS

- Aldridge, B. B., J. Saez-Rodriguez, J. L. Muhlich, P. K. Sorger and D. A. Lauffenburger (2009). "Fuzzy Logic Analysis of Kinase Pathway Crosstalk in TNF/EGF/Insulin-Induced Signaling." PLoS Comput Biol **5**(4): e1000340.
- Alexander, W. S. (2002). "Suppressors of cytokine signalling (SOCS) in the immune system." Nat Rev Immunol **2**(6): 410-6.
- Anderson, P. (2010). "Post-transcriptional regulons coordinate the initiation and resolution of inflammation." Nat Rev Immunol **10**(1): 24-35.
- Balachandran, S., P. C. Roberts, L. E. Brown, H. Truong, A. K. Pattnaik, D. R. Archer and G. N. Barber (2000). "Essential role for the dsRNA-dependent protein kinase PKR in innate immunity to viral infection." Immunity **13**(1): 129-41.
- Bandyopadhyay, S. K., D. V. Kalvakolanu and G. C. Sen (1990). "Gene induction by interferons: functional complementation between trans-acting factors induced by alpha interferon and gamma interferon." Mol Cell Biol **10**(10): 5055-63.
- Banninger, G. and N. C. Reich (2004). "STAT2 nuclear trafficking." J Biol Chem **279**(38): 39199-206.
- Barua, D., J. R. Faeder and J. M. Haugh (2007). "Structure-based kinetic models of modular signaling protein function: focus on Shp2." Biophys J **92**(7): 2290-300.
- Battiti, R. (1992). "First- and Second-Order Methods for Learning: Between Steepest Descent and Newton's Method." Neural Computation **4**(2): 141-166.

Citations

- Becker, V., M. Schilling, J. Bachmann, U. Baumann, A. Raue, T. Maiwald, J. Timmer and U. Klingmüller (2010). "Covering a Broad Dynamic Range: Information Processing at the Erythropoietin Receptor." Science **328**(5984): 1404-1408.
- Behar, M. and A. Hoffmann (2010). "Understanding the temporal codes of intra-cellular signals." Current Opinion in Genetics & Development **20**(6): 684-693.
- Chen, L., I. Borozan, J. Feld, J. Sun, L. L. Tannis, C. Coltescu, J. Heathcote, A. M. Edwards and I. D. McGilvray (2005). "Hepatic gene expression discriminates responders and nonresponders in treatment of chronic hepatitis C viral infection." Gastroenterology **128**(5): 1437-44.
- Chen, W. W., M. Niepel and P. K. Sorger (2010). "Classic and contemporary approaches to modeling biochemical reactions." Genes & Development **24**(17): 1861-1875.
- Chung, C. D., J. Liao, B. Liu, X. Rao, P. Jay, P. Berta and K. Shuai (1997). "Specific inhibition of Stat3 signal transduction by PIAS3." Science **278**(5344): 1803-5.
- Crocker, B. A., H. Kiu and S. E. Nicholson (2008). "SOCS regulation of the JAK/STAT signalling pathway." Semin Cell Dev Biol **19**(4): 414-22.
- Der, S. D., A. Zhou, B. R. Williams and R. H. Silverman (1998). "Identification of genes differentially regulated by interferon alpha, beta, or gamma using oligonucleotide arrays." Proc Natl Acad Sci U S A **95**(26): 15623-8.
- Dokoumetzidis, A. and L. Aarons (2009). "Proper lumping in systems biology models." IET Systems Biology **3**(1): 40-51.
- Frearson, J. A. and D. R. Alexander (1997). "The role of phosphotyrosine phosphatases in haematopoietic cell signal transduction." Bioessays **19**(5): 417-27.

Citations

- Frontini, M., M. Vijayakumar, A. Garvin and N. Clarke (2009). "A ChIP-chip approach reveals a novel role for transcription factor IRF1 in the DNA damage response." Nucleic Acids Research **37**(4): 1073-1085.
- Gavutis, M., E. Jaks, P. Lamken and J. Piehler (2006). "Determination of the two-dimensional interaction rate constants of a cytokine receptor complex." Biophys J **90**(9): 3345-55.
- Guhaniyogi, J. and G. Brewer (2001). "Regulation of mRNA stability in mammalian cells." Gene **265**(1-2): 11-23.
- Gutenkunst, R. N., J. J. Waterfall, F. P. Casey, K. S. Brown, C. R. Myers and J. P. Sethna (2007). "Universally sloppy parameter sensitivities in systems biology models." PLoS Comput Biol **3**(10): 1871-78.
- Hao, S. and D. Baltimore (2009). "The stability of mRNA influences the temporal order of the induction of genes encoding inflammatory molecules." Nat Immunol **10**(3): 281-288.
- Harman, A. N., J. Lai, S. Turville, S. Samarajiwa, L. Gray, V. Marsden, S. Mercier, K. Jones, N. Nasr, A. Rustagi, H. Cumming, H. Donaghy, J. Mak, M. Gale, Jr., M. Churchill, P. Hertzog and A. L. Cunningham (2011). "HIV infection of dendritic cells subverts the IFN induction pathway via IRF-1 and inhibits type 1 IFN production." Blood **118**(2): 298-308.
- Heinrich, R., B. G. Neel and T. A. Rapoport (2002). "Mathematical models of protein kinase signal transduction." Mol Cell **9**(5): 957-70.
- Hood, L. and S. H. Friend (2011). "Predictive, personalized, preventive, participatory (P4) cancer medicine." Nat Rev Clin Oncol **8**(3): 184-187.
- Hoops, S., S. Sahle, R. Gauges, C. Lee, J. Pahle, N. Simus, M. Singhal, L. Xu, P. Mendes and U. Kummer (2006). "COPASI--a COmplex PAthway SIMulator." Bioinformatics **22**(24): 3067-74.

Citations

- Hornberg, J. J., B. Binder, F. J. Bruggeman, B. Schoeberl, R. Heinrich and H. V. Westerhoff (2005). "Control of MAPK signalling: from complexity to what really matters." Oncogene **24**(36): 5533-42.
- Huang, D. W., B. T. Sherman and R. A. Lempicki (2008). "Systematic and integrative analysis of large gene lists using DAVID bioinformatics resources." Nat. Protocols **4**(1): 44-57.
- Hucka, M., A. Finney, H. M. Sauro, H. Bolouri, J. C. Doyle, H. Kitano, S. F. and the rest of the, A. P. Arkin, B. J. Bornstein, D. Bray, A. Cornish-Bowden, A. A. Cuellar, S. Dronov, E. D. Gilles, M. Ginkel, V. Gor, I. I. Goryanin, W. J. Hedley, T. C. Hodgman, J. H. Hofmeyr, P. J. Hunter, N. S. Juty, J. L. Kasberger, A. Kremling, U. Kummer, N. Le NovÃ´re, L. M. Loew, D. Lucio, P. Mendes, E. Minch, E. D. Mjolsness, Y. Nakayama, M. R. Nelson, P. F. Nielsen, T. Sakurada, J. C. Schaff, B. E. Shapiro, T. S. Shimizu, H. D. Spence, J. Stelling, K. Takahashi, M. Tomita, J. Wagner and J. Wang (2003). "The systems biology markup language (SBML): a medium for representation and exchange of biochemical network models." Bioinformatics **19**(4): 524-531.
- Isaacs, A. and J. Lindenmann (1957). "Virus Interference. I. The Interferon." Proceedings of the Royal Society of London. Series B - Biological Sciences **147**(927): 258-267.
- Jaks, E., M. Gavutis, G. Uze, J. Martal and J. Piehler (2007). "Differential receptor subunit affinities of type I interferons govern differential signal activation." J Mol Biol **366**(2): 525-39.
- Jaqaman, K. and G. Danuser (2006). "Linking data to models: data regression." Nat Rev Mol Cell Biol **7**(11): 813-819.
- Kalvakolanu V, D. (2003). "Alternate interferon signaling pathways." Pharmacology & Therapeutics **100**(1): 1-29.

Citations

- Kile, B. T., B. A. Schulman, W. S. Alexander, N. A. Nicola, H. M. Martin and D. J. Hilton (2002). "The SOCS box: a tale of destruction and degradation." Trends Biochem Sci **27**(5): 235-41.
- Kitano, H. (2002a). "Computational systems biology." Nature **420**(6912): 206-210.
- Kitano, H. (2002b). "Systems Biology: A Brief Overview." Science **295**(5560): 1662-1664.
- Kitano, H., A. Funahashi, Y. Matsuoka and K. Oda (2005). "Using process diagrams for the graphical representation of biological networks." Nat Biotechnol **23**(8): 961-6.
- Koromilas, A. E., S. Li and G. Matlashewski (2001). "Control of interferon signaling in human papillomavirus infection." Cytokine Growth Factor Rev **12**(2-3): 157-70.
- Lau, J. F., J. P. Parisien and C. M. Horvath (2000). "Interferon regulatory factor subcellular localization is determined by a bipartite nuclear localization signal in the DNA-binding domain and interaction with cytoplasmic retention factors." Proc Natl Acad Sci U S A **97**(13): 7278-83.
- Leonard, G. T. and G. C. Sen (1997). "Restoration of interferon responses of adenovirus E1A-expressing HT1080 cell lines by overexpression of p48 protein." J Virol **71**(7): 5095-101.
- Levy, D. E. and J. E. Darnell, Jr. (2002). "Stats: transcriptional control and biological impact." Nat Rev Mol Cell Biol **3**(9): 651-62.
- Levy, D. E., D. J. Lew, T. Decker, D. S. Kessler and J. E. Darnell, Jr. (1990). "Synergistic interaction between interferon-alpha and interferon-gamma through induced synthesis of one subunit of the transcription factor ISGF3." EMBO J **9**(4): 1105-11.
- Li, X., S. Leung, S. Qureshi, J. E. Darnell and G. R. Stark (1996). "Formation of STAT1-STAT2 Heterodimers and Their Role in the Activation of IRF-1 Gene Transcription by Interferon." Journal of Biological Chemistry **271**(10): 5790-5794.

Citations

- Maiwald, T., A. Schneider, H. Busch, S. Sahle, N. Gretz, T. S. Weiss, U. Kummer and U. Klingmuller (2010). "Combining theoretical analysis and experimental data generation reveals IRF9 as a crucial factor for accelerating interferon alpha-induced early antiviral signalling." FEBS J **277**(22): 4741-54.
- Maiwald, T. and J. Timmer (2008). "Dynamical modeling and multi-experiment fitting with PottersWheel." Bioinformatics **24**(18): 2037-2043.
- Malakhov, M. P., O. A. Malakhova, K. I. Kim, K. J. Ritchie and D. E. Zhang (2002). "UBP43 (USP18) specifically removes ISG15 from conjugated proteins." J Biol Chem **277**(12): 9976-81.
- Malakhova, O. A., K. I. Kim, J. K. Luo, W. Zou, K. G. Kumar, S. Y. Fuchs, K. Shuai and D. E. Zhang (2006). "UBP43 is a novel regulator of interferon signaling independent of its ISG15 isopeptidase activity." EMBO J **25**(11): 2358-67.
- Manns, M. P., J. G. McHutchison, S. C. Gordon, V. K. Rustgi, M. Shiffman, R. Reindollar, Z. D. Goodman, K. Koury, M. Ling and J. K. Albrecht (2001). "Peginterferon alfa-2b plus ribavirin compared with interferon alfa-2b plus ribavirin for initial treatment of chronic hepatitis C: a randomised trial." Lancet **358**(9286): 958-65.
- Marquardt, D. W. (1963). "An Algorithm for Least-Squares Estimation of Nonlinear Parameters." SIAM Journal on Applied Mathematics **11**(2): 431-441.
- Martinez-Moczygemba, M., M. J. Gutch, D. L. French and N. C. Reich (1997). "Distinct STAT structure promotes interaction of STAT2 with the p48 subunit of the interferon-alpha-stimulated transcription factor ISGF3." J Biol Chem **272**(32): 20070-6.
- Meyer, T., A. Marg, P. Lemke, B. Wiesner and U. Vinkemeier (2003). "DNA binding controls inactivation and nuclear accumulation of the transcription factor Stat1." Genes Dev **17**(16): 1992-2005.

Citations

O'Shea, J. J. and W. Watford (2004). "A peek at PIAS." Nat Immunol **5**(9): 875-876.

Onoguchi, K., M. Yoneyama, A. Takemura, S. Akira, T. Taniguchi, H. Namiki and T. Fujita (2007). "Viral infections activate types I and III interferon genes through a common mechanism." J Biol Chem **282**(10): 7576-81.

Petzold, L. (1983). "Automatic Selection of Methods for Solving Stiff and Nonstiff Systems of Ordinary Differential Equations." SIAM J Sci And Stat Comput **4**(1): 136-148.

Pitha, P. M. (2011). "Innate Antiviral Response: Role in HIV-1 Infection." Viruses **3**(7): 1179-1203.

Platanias, L. C. (2005). "Mechanisms of type-I- and type-II-interferon-mediated signalling." Nat Rev Immunol **5**(5): 375-86.

Randall, R. E. and S. Goodbourn (2008). "Interferons and viruses: an interplay between induction, signalling, antiviral responses and virus countermeasures." J Gen Virol **89**(Pt 1): 1-47.

Rateitschak, K., A. Karger, B. Fitzner, F. Lange, O. Wolkenhauer and R. Jaster (2009). "Mathematical modelling of interferon-gamma signalling in pancreatic stellate cells reflects and predicts the dynamics of STAT1 pathway activity." Cell Signal **22**(1): 97-105.

Raue, A., C. Kreutz, T. Maiwald, J. Bachmann, M. Schilling, U. Klingmüller and J. Timmer (2009). "Structural and practical identifiability analysis of partially observed dynamical models by exploiting the profile likelihood." Bioinformatics **25**(15): 1923-1929.

Raue, A., C. Kreutz, T. Maiwald, U. Klingmüller and J. Timmer (2011). "Addressing parameter identifiability by model-based experimentation." IET Systems Biology **5**(2): 120-130.

Citations

- Reich, N. C. (2007). "STAT dynamics." Cytokine Growth Factor Rev **18**(5-6): 511-8.
- Reich, N. C. and L. Liu (2006). "Tracking STAT nuclear traffic." Nat Rev Immunol **6**(8): 602-12.
- Sahle, S., P. Mendes, S. Hoops and U. Kummer (2008). "A new strategy for assessing sensitivities in biochemical models." Philosophical Transactions of the Royal Society A: Mathematical, Physical and Engineering Sciences **366**(1880): 3619-3631.
- Sarasin-Filipowicz, M., E. J. Oakeley, F. H. Duong, V. Christen, L. Terracciano, W. Filipowicz and M. H. Heim (2008). "Interferon signaling and treatment outcome in chronic hepatitis C." Proc Natl Acad Sci U S A **105**(19): 7034-9.
- Sarasin-Filipowicz, M., X. Wang, M. Yan, F. H. Duong, V. Poli, D. J. Hilton, D. E. Zhang and M. H. Heim (2009). "Alpha interferon induces long-lasting refractoriness of JAK-STAT signaling in the mouse liver through induction of USP18/UBP43." Mol Cell Biol **29**(17): 4841-51.
- Schoeberl, B., C. Eichler-Jonsson, E. D. Gilles and G. Muller (2002). "Computational modeling of the dynamics of the MAP kinase cascade activated by surface and internalized EGF receptors." Nat Biotech **20**(4): 370-375.
- Schoggins, J. W., S. J. Wilson, M. Panis, M. Y. Murphy, C. T. Jones, P. Bieniasz and C. M. Rice (2011). "A diverse range of gene products are effectors of the type I interferon antiviral response." Nature **472**(7344): 481-485.
- Shuai, K. (2006). "Regulation of cytokine signaling pathways by PIAS proteins." Cell Res **16**(2): 196-202.
- Shuai, K. and B. Liu (2003). "Regulation of JAK-STAT signalling in the immune system." Nat Rev Immunol **3**(11): 900-11.

Citations

- Shvartsman, S. Y., M. P. Hagan, A. Yacoub, P. Dent, H. S. Wiley and D. A. Lauffenburger (2002). "Autocrine loops with positive feedback enable context-dependent cell signaling." *American Journal of Physiology - Cell Physiology* **282**(3): C545-C559.
- Smieja, J., M. Jamaluddin, A. R. Brasier and M. Kimmel (2008). "Model-based analysis of interferon-beta induced signaling pathway." *Bioinformatics* **24**(20): 2363-9.
- Snijder, B., R. Sacher, P. Ramo, E.-M. Damm, P. Liberali and L. Pelkmans (2009). "Population context determines cell-to-cell variability in endocytosis and virus infection." *Nature* **461**(7263): 520-523.
- Stark, G. R., I. M. Kerr, B. R. Williams, R. H. Silverman and R. D. Schreiber (1998). "How cells respond to interferons." *Annu Rev Biochem* **67**: 227-64.
- Stirnweiss, A., A. Ksienzyk, K. Klages, U. Rand, M. Grashoff, H. Hauser and A. Kröger (2010). "IFN Regulatory Factor-1 Bypasses IFN-Mediated Antiviral Effects through Viperin Gene Induction." *The Journal of Immunology* **184**(9): 5179-5185.
- Surovtsova, I., N. Simus, T. Lorenz, A. König, S. Sahle and U. Kummer (2009). "Accessible methods for the dynamic time-scale decomposition of biochemical systems." *Bioinformatics* **25**(21): 2816-2823.
- Szklarczyk, D., A. Franceschini, M. Kuhn, M. Simonovic, A. Roth, P. Minguéz, T. Doerks, M. Stark, J. Müller, P. Bork, L. J. Jensen and C. v. Mering (2011). "The STRING database in 2011: functional interaction networks of proteins, globally integrated and scored." *Nucleic Acids Research* **39**(suppl 1): D561-D568.
- Tamada, Y., K. Nakao, Y. Nagayama, K. Nakata, T. Ichikawa, Y. Kawamata, H. Ishikawa, K. Hamasaki, K. Eguchi and N. Ishii (2002). "p48 Overexpression enhances interferon-mediated expression and activity of double-stranded RNA-dependent protein kinase in human hepatoma cells." *J Hepatol* **37**(4): 493-9.

Citations

- ten Hoeve, J., M. de Jesus Ibarra-Sanchez, Y. Fu, W. Zhu, M. Tremblay, M. David and K. Shuai (2002). "Identification of a Nuclear Stat1 Protein Tyrosine Phosphatase." Mol. Cell. Biol. **22**(16): 5662-5668.
- Terenzi, F., P. Saikia and G. C. Sen (2008). "Interferon-inducible protein, P56, inhibits HPV DNA replication by binding to the viral protein E1." EMBO J **27**(24): 3311-21.
- Versteeg, G. A. and A. Garcia-Sastre (2010). "Viral tricks to grid-lock the type I interferon system." Curr Opin Microbiol **13**(4): 508-16.
- Vinkemeier, U. (2004). "Getting the message across, STAT! Design principles of a molecular signaling circuit." The Journal of Cell Biology **167**(2): 197-201.
- Weihua, X., J. Hu, S. K. Roy, S. B. Mannino and D. V. Kalvakolanu (2000). "Interleukin-6 modulates interferon-regulated gene expression by inducing the ISGF3 gamma gene using CCAAT/enhancer binding protein-beta(C/EBP-beta)." Biochim Biophys Acta **1492**(1): 163-71.
- Wesoly, J., Z. Szweykowska-Kulinska and H. A. Bluysen (2007). "STAT activation and differential complex formation dictate selectivity of interferon responses." Acta Biochim Pol **54**(1): 27-38.
- Yamada, S., S. Shiono, A. Joo and A. Yoshimura (2003). "Control mechanism of JAK/STAT signal transduction pathway." FEBS Lett **534**(1-3): 190-6.
- You, M., D.-H. Yu and G.-S. Feng (1999). "Shp-2 Tyrosine Phosphatase Functions as a Negative Regulator of the Interferon-Stimulated Jak/STAT Pathway." Mol. Cell. Biol. **19**(3): 2416-2424.
- Zaslavsky, E., U. Hershberg, J. Seto, A. M. Pham, S. Marquez, J. L. Duke, J. G. Wetmur, B. R. tenOever, S. C. Sealfon and S. H. Kleinstein (2010). "Antiviral Response Dictated by

Citations

Choreographed Cascade of Transcription Factors." The Journal of Immunology **184**(6): 2908-2917.

Zi, Z., K. H. Cho, M. H. Sung, X. Xia, J. Zheng and Z. Sun (2005). "In silico identification of the key components and steps in IFN-gamma induced JAK-STAT signaling pathway." FEBS Lett **579**(5): 1101-8.

ERKLÄRUNG

Ich erkläre hiermit, dass ich die vorgelegte Dissertation selbst verfasst und mich dabei keiner anderen als der von mir ausdrücklich bezeichneten Quellen und Hilfen bedient habe.

Weiterhin erkläre ich hiermit, dass ich an keiner anderen Stelle ein Prüfungsverfahren beantragt bzw. die Dissertation in dieser oder anderer Form bereits anderweitig als Prüfungsarbeit verwendet oder einer anderen Fakultät als Dissertation vorgelegt habe.

Heidelberg, den 21. Dezember 2011